CHAPTER

NR WAVEFORM

6

CP-OFDM waveform has been widely adopted for wireless and wireline communication as well as for digital audio and video broadcasting. The Asymmetric Digital Subscriber Line (ADSL) was the first wireline technology that used OFDM for high speed transmission. Digital Audio Broadcasting (DAB) and Digital Video Broadcasting (DVB-T) standards employ OFDM for broadcasting digital audio and video services. Various wireless IEEE and 3GPP standards have adopted OFDM, for example, IEEE 802.11a/WLAN, IEEE 802.16/WiMAX, 3GPP 4G LTE, and more recently 3GPP 5G NR. In this chapter, we discuss the OFDM design for 5G NR.

This chapter is organized as follows. Section 6.1 discusses suitability of CP-OFDM for NR. Section 6.2 describes a scalable OFDM design for NR, as adopted by the 3GPP. Section 6.3 provides a detailed discussion of how the scalable parameters of OFDM should be chosen considering various factors such as quality of service requirements, type of deployment, carrier frequency, user mobility, hardware impairments, and implementation aspects. Section 6.4 discusses the need for improving power efficiency of the NR waveform for coverage limited scenarios, along with a brief overview of the commonly used techniques. The effects of different synchronization errors in a CP-OFDM system are discussed in Section 6.5. Finally, some mitigation techniques for the hardware impairments (phase noise, carrier-frequency offset, and sampling frequency offset) are presented in Section 6.6.

6.1 SUITABILITY OF OFDM FOR NR

For the NR waveform, the design requirements vary depending on the carrier-frequency range and the link type, as discussed in Chapter 5. The 3GPP has selected CP-OFDM waveform for NR after a thorough investigation of several multicarrier and single-carrier waveforms considering requirements that are important for the NR design. In Chapter 5, we have also provided a comparison of state-of-the art waveforms. In the following, we discuss the suitability of OFDM for NR for various link types (uplink, downlink, sidelink,[1] vehicle-to-anything (V2X)[2] link, backhaul link) considering the waveform key performance indicators:

- ***Spectral efficiency*** OFDM is well known for its high spectral efficiency. The spectral efficiency is vital to meet extreme data rate requirements with NR. In general, the spectral efficiency is more crucial at lower carrier frequencies than at higher frequencies due to potentially much larger channel bandwidths at higher carrier frequencies. The spectral efficiency is important for both uplink and

[1] Sidelink refers to direct device-to-device (D2D) communication.

[2] Vehicle-to-anything (V2X) communication includes vehicle-to-vehicle (V2V), vehicle-to-infrastructure (V2I), vehicle-to-network (V2N), and vehicle-to-pedestrian (V2P).

5G Physical Layer. https://doi.org/10.1016/B978-0-12-814578-4.00011-4

the downlink. The requirements are even more stringent for the backhaul link due to the massive volumes of data transmission between the base stations. Vehicular communication can also create capacity bottlenecks in dense urban scenarios with large number of vehicles periodically broadcasting signals in an asynchronous fashion.

- ***MIMO compatibility*** OFDM enables a straightforward use of MIMO technology (see Chapter 7). With increase in the carrier frequency with NR, the number of antenna elements would increase in the base stations as well as in the devices. The use of various MIMO schemes is essential for enhancing spectral efficiency by enabling SU-MIMO/MU-MIMO and achieving greater coverage via beam-forming (see Chapter 7). Beam-forming is instrumental in overcoming high propagation losses at very high frequencies where coverage is limited.
- ***Peak-to-Average-Power-Ratio (PAPR)*** OFDM has a high PAPR like other multicarrier waveforms (see Section 5.5.2). A low PAPR is essential for power-efficient transmissions from the devices (for example, in the uplink and the sidelink). A low PAPR becomes even more important at very high frequencies where coverage can be limited. It is noteworthy that small sized low cost base stations are envisioned at high frequencies, therefore, low PAPR is also important for the downlink transmissions at high carrier frequencies. A high PAPR in OFDM can also be substantially reduced via various well-known PAPR reduction techniques with only minor compromise in performance [10] (see Section 6.4). For NR, OFDM with PAPR reduction is an attractive option for the uplink and the sidelink.

  LTE uses DFTS-OFDM for both uplink and sidelink due to its lower PAPR. However, DFTS-OFDM has certain drawbacks in comparison with OFDM such as lesser flexibility for scheduling and more complex MIMO receiver with degraded link level and system level performance [21]. For NR, DFTS-OFDM is optional for the uplink and can be used only for a single-stream (without MIMO) transmission. Since MIMO transmission is a key component of NR, DFTS-OFDM is not a preferred option for the uplink and the sidelink in general. The use of one waveform (i.e., OFDM) for all link types also makes transceiver designs and implementations symmetric for all transmissions.
- ***Robustness to channel time selectivity*** is vital in high mobility scenarios. High-speed UEs are relevant in large cell deployments. The large cell deployments are not expected at very high frequencies due to harsh propagation conditions (coverage limitation). At very high frequencies, the deployments are expected in the form of small cells where mobility is not a major concern. However, the V2V services may be enabled at very high frequencies, making robustness to the channel time selectivity a very important performance indicator at very high frequencies. Traditionally, the backhaul link is fixed and mobility is not a concern, however, for the envisioned mobile backhaul (e.g., access nodes on vehicles), robustness to channel time selectivity will become relevant. OFDM can be made robust to channel time selectivity by a proper choice of the subcarrier spacing.
- ***Robustness to channel frequency selectivity*** Channel frequency selectivity is always relevant to the transmission of large bandwidth signals over wireless multipath channels. Channel frequency selectivity depends on various factors such as the type of deployment, the beam-forming technique, and the signal bandwidth. OFDM is robust to frequency-selective channels and requires only single-tap frequency-domain equalization.
- ***Robustness against phase noise*** Typically, phase-noise increases with an increase in the oscillator frequency (see Section 4.2). An OFDM system can be made robust to phase-noise by a proper choice of its subcarrier spacing (see Section 6.3.1). Phase-noise robustness is crucial for all link types where a UE (transmitter/receiver) is involved. In particular, low phase-noise oscillators may be

too expensive and power consuming for devices (UEs). Phase-noise robustness is also important for future low cost base stations. Basically, any link that involves a device and/or a low cost base station puts a high requirement on phase-noise robustness of the waveform, especially if the communication takes place at high carrier frequencies.

- ***Transceiver baseband complexity*** The baseband complexity of an OFDM receiver is lowest among all 5G candidate waveforms as discussed in Chapter 5 (see Section 5.5.4 for a complexity comparison). The baseband complexity is always very important at the device (UE) side, especially from the receiver perspective. For NR, the baseband complexity is also a major consideration for the base stations, since an NR base station can be a small sized access node (especially at high frequencies) with a limited processing capability. At very high frequencies and large bandwidths, the receiver also has to cope with severe RF impairments.
- ***Time localization*** OFDM is very well localized in the time domain, which is important to efficiently enable (dynamic) TDD and support latency critical applications such as URLLC (see Section 2.7). Dynamic TDD is envisioned at high frequencies and provision of low latency is essential for all link types; especially backhaul and V2V links may impose very high requirements.
- ***Frequency localization*** OFDM is less localized in the frequency domain (see Section 5.5.1). Frequency localization can be relevant to support the coexistence of different services potentially enabled by mixing different waveform numerologies in the frequency domain on the same carrier (see Section 6.3.3). Frequency localization is also relevant if asynchronous access is allowed in uplink and sidelink. In general, frequency localization of a waveform may not be crucial at high frequencies where large channel bandwidths are available.
- ***Robustness to synchronization errors*** The provision of the cyclic prefix in OFDM makes it robust to timing synchronization errors (see Section 6.5.1). Robustness to the synchronization errors is relevant in scenarios where the synchronization is hard to achieve such as in the sidelink. It can also be important if asynchronous transmissions are allowed in the uplink.[3]
- ***Flexibility and scalability*** OFDM is a flexible waveform which can support diverse services in a wide range of frequencies by a proper choice of the subcarrier spacing and the cyclic prefix. (See Section 6.2 for a discussion on the OFDM numerology design that fulfills a wide range of requirements for NR.)

A summary of the waveform design requirements for different link types is shown in Fig. 6.1. A link requirement "High" for a waveform KPI tells that the given KPI is important for the given link type in general. Furthermore, a high-level assessment of OFDM is given in Table 6.1. The OFDM assessment "High" means that OFDM has good performance in general for the given KPI. We assess the D2D and V2V cases separately due to different levels of requirements. For example, V2V communication has higher requirements on the mobility and the system capacity, whereas there are lower requirements on the power efficiency when compared with UE-to-UE communication. Based on the overall assessment, it can be concluded that OFDM is an excellent choice for the NR air interface for all link types.

[3]We note that LTE only supports synchronous uplink transmission, which is realized via a timing advance mechanism at the UEs.

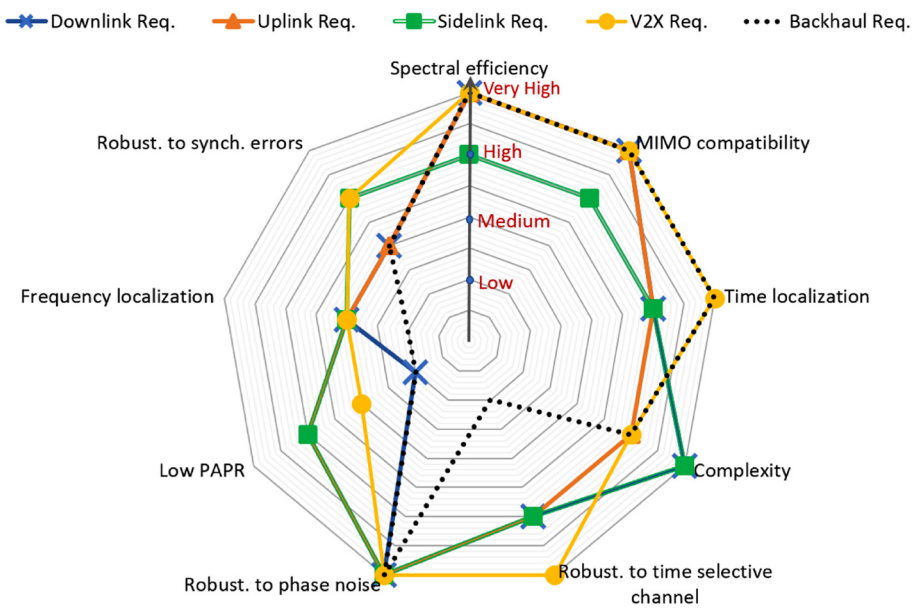

FIGURE 6.1

A high-level summary of the waveform design requirements for different link types: uplink, downlink, sidelink, V2V link, and backhaul link.

Table 6.1 A high-level assessment of OFDM

Performance indicators	OFDM assessment
Spectral efficiency	High
MIMO compatibility	High
Time localization	High
Transceiver baseband complexity	Low
Flexibility/Scalability	High
Robust. to freq.-selective chan.	High
Robust. to time-selective chan.	Medium
Medium Robust. to phase noise	Medium
Robust. to synch. errors	Medium
PAPR	High (can be improved)
Frequency localization	Low (can be improved)

6.2 SCALABLE OFDM FOR NR

CP-OFDM waveform has a few design parameters: subcarrier spacing, cyclic prefix, and the number of subcarriers. For a communication system, these parameters can be optimized based on a number of factors including carrier frequency, user mobility, phase noise, channel delay spread, quality of service

Table 6.2 Scalable OFDM numerology for 5G NR

OFDM subcarrier spacing	15 kHz	30 kHz	60 kHz	15×2^n kHz ($n \geq 3$)
OFDM symbol duration	66.67 μs	33.33 μs	16.67 μs	$66.67/2^n$ μs
Cyclic-prefix duration	4.69 μs	2.34 μs	1.17 μs	$4.69/2^n$ μs
OFDM symbol with CP	71.35 μs	35.68 μs	17.84 μs	$71.35/2^n$ μs
OFDM symbols per slot	14	14	14	14
Slot duration	1000 μs	500 μs	250 μs	$1000/2^n$ μs

Numerologies with $n = \{-2, -1\}$ are possible but not listed in this table.

requirements, signal bandwidth, and implementation complexity. For a given carrier frequency, phase noise and the Doppler effect set requirements on the minimum subcarrier spacing. The use of smaller subcarrier spacings either results in a high error vector magnitude (EVM) due to phase noise or in undesirable strict requirements on the local oscillator. Too narrow subcarrier spacings lead to performance degradations in high Doppler effect scenarios. The required cyclic-prefix overhead (and thus anticipated delay spread) sets an upper limit for the subcarrier spacing; selecting larger subcarriers would result in an undesirable high CP overhead (degrading spectral efficiency). The maximum FFT size of the OFDM modulator (or the number of total subcarriers) together with subcarrier spacing determines the channel bandwidth. Based on these relationships, the subcarrier spacing is typically chosen as small as possible while still being robust against phase noise and Doppler effect and providing the desired channel bandwidth. These design principles also apply to NR, as we will discuss in the sequel.

NR will operate from sub-1 GHz to 100 GHz using a wide range of deployment options (e.g., macro cells, micro cells, pico cells). Furthermore, NR will cover a very wide application range, including mobile broadband and several types of machine type communications. A single OFDM numerology cannot fulfill the desired frequency range and all envisioned deployment options and applications; therefore, the 3GPP has adopted a family of OFDM numerologies for NR. In the 3GPP context, OFDM numerology refers to the choice of OFDM subcarrier spacing, cyclic-prefix duration, and the number of OFDM symbols per transmission slot.[4] In particular, it has been agreed that the subcarrier spacing of OFDM can be chosen according to 15×2^n kHz, where n is an integer-valued parameter and the cyclic-prefix overhead is 7% as in LTE. The details related to NR OFDM numerologies (as agreed in the 3GPP) such as CP duration, symbol duration, and slot size, are given in Table 6.2. (We note that in 3GPP NR Release 15, the numerology is specified for up to 52.6 GHz carrier frequency with 120 kHz as the maximum subcarrier spacing as given in Table 2.1.[5]) The 15 kHz numerology is exactly the same as in LTE, with a minor exception that in LTE a slot contains seven OFDM symbols whereas a slot in NR has 14 OFDM symbols. For all numerologies, the cyclic prefix of the first OFDM symbol in every 0.5 ms interval is 16 T_s ($T_s = 32.6$ ns is the chip duration corresponding to an LTE sampling rate of 30.72 MHz) longer than the cyclic prefix of the remaining OFDM symbols in the interval. This implies that a slot length can slightly vary, depending on where it starts.

[4] See Section 2.3 for definition of the slot in NR.

[5] In 3GPP NR Release 15, the OFDM numerology is not specified for the frequency range 6 GHz to 24 GHz, since no spectrum has been identified for NR in this range. When the spectrum becomes available in the future, the numerology can be specified.

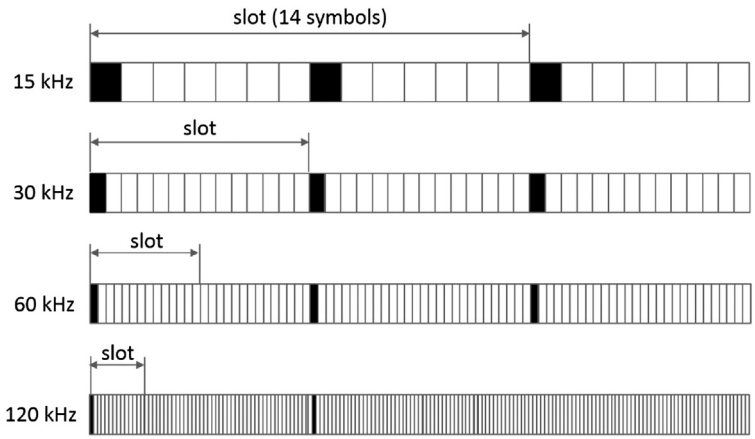

FIGURE 6.2

The NR numerology ensures symbol-wise and slot-wise time alignment. The time alignment is important for efficiently enabling TDD networks.

Fig. 6.2 illustrates OFDM symbols and slots for different numerologies (15 kHz, 30 kHz, 60 kHz, and 120 kHz), where symbols with darker colors represent OFDM symbols with longer CPs (every 0.5 ms). We observe that an integer number of slots of one numerology (with wider subcarrier spacing) fits into a slot of another numerology (with narrower subcarrier spacing). This time alignment of the slots is important for TDD networks to allow for time-aligned uplink and downlink transmission periods, which is discussed further in Section 6.2.2.

The 3GPP has introduced the concept of mini-slots in NR to support transmissions shorter than regular slot duration (see Section 2.3). A mini-slot can start at any OFDM symbol in a regular slot. Mini-slots can be useful in various scenarios—three important utilizations are shown in Fig. 6.3: i) low-latency transmissions, where the regular slot duration is too long and/or a transmission need to start immediately without waiting for the start of a slot boundary, ii) transmissions in an unlicensed spectrum, where it is beneficial to start transmission immediately after LBT, and iii) transmission in the millimeter-wave band, where the large channel bandwidths imply that the payload supported by one or two OFDM symbols can be sufficient for many of the packets. Furthermore, in the millimeter wave band the multiplexing of different users should primarily be done in the time domain to support analog/hybrid beam-forming, calling for a transmission duration shorted than a slot.

In principle, a mini-slot for a numerology can be as short as one OFDM symbol.[6] Some desirable characteristics of the mini-slot are: a mini-slot should be aligned with OFDM symbol boundaries in the regular slot; a mini-slot should end at the slot boundaries at latest; it should be possible to aggregate a mini-slot with a subsequent slot; and it may either contain control information at its beginning or at its end.

[6] In 3GPP NR Release 15, the downlink mini-slots are restricted to 2, 4, and 7 OFDM symbols.

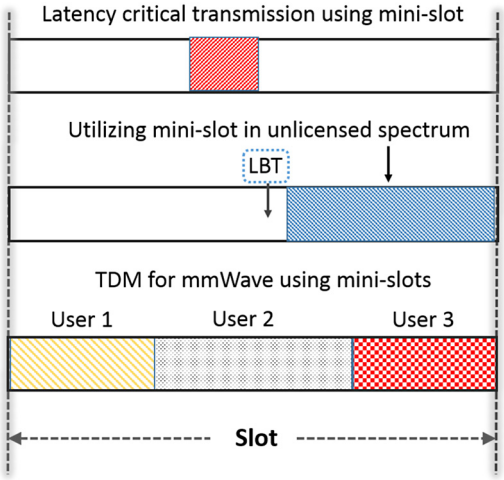

FIGURE 6.3

Mini-slots are useful in various situations, e.g., to achieve low latency, to efficiently transmit in an unlicensed spectrum based on listen-before-talk, and to schedule users at shorter time scales in the millimeter-wave band where large channel bandwidths are available.

6.2.1 WHY 15 KHZ AS BASELINE NUMEROLOGY?

The LTE OFDM numerology is 15 kHz subcarrier spacing with 7% cyclic-prefix overhead (4.69 μs). The numerology for LTE was specified after a thorough investigation in the 3GPP. For NR, it was straightforward for the 3GPP to aim for a similar OFDM numerology at LTE-like frequencies and deployments. Different subcarrier spacing options close to 15 kHz were therefore considered by the 3GPP as a baseline numerology for NR. The conclusion is to keep the LTE numerology as the baseline numerology for NR. There are two important reasons for keeping the LTE numerology as the base numerology:

- Narrow Band-IoT (NB-IoT) is a new radio access technology (already deployed since 2017) to support massive machine-type communications. NB-IoT uses the LTE numerology and provides different deployments, among others, an in-band deployment within an LTE carrier that is enabled by the selected LTE numerology. NB-IoT devices are designed to operate for 10 years or more on a single battery charge. Once such an NB-IoT device is deployed it is likely that within the device life time the embedding carrier (assuming in-band LTE deployment) gets refarmed to NR. The main reason for selecting the LTE-based numerology for NB-IoT was the option of the in-band deployment; in-band NB-IoT deployments after refarming LTE to NR would benefit from the LTE-based numerology.
- NR deployments can happen in the same band as LTE. With an adjacent LTE TDD carrier, NR must adopt the same uplink/downlink switching pattern as the LTE TDD does. Every numerology where (an integer multiple of) a subframe is 1 ms can be aligned with regular subframes in LTE. In LTE, the duplex switching happens in special subframes. To match the transmission direction in the special subframes, the same numerology as in LTE is needed.

The above arguments together with LTE numerology proven in the field were strong enough to set the baseline OFDM numerology for NR to the LTE numerology (to be used in LTE-like frequencies and deployments). This implies the same subcarrier spacing (15 kHz), the same OFDM symbol duration (66.67 μs), and the same cyclic prefix (4.69 μs).

6.2.2 WHY 15×2^n KHZ SCALING?

As discussed earlier, a set of OFDM numerologies had to be defined for NR to handle a wide range of frequencies and deployment options. These OFDM numerologies could either be unrelated to each other, i.e., the OFDM numerology for a given frequency and deployment is only based on this frequency and deployment, not considering numerologies for other frequencies and deployments at all. Another option was to define a family of OFDM numerologies which are related to each other via scaling, i.e.,

$$\Delta f_i = n_i \Delta f_{i-1}, \quad T_{cp,(i)} = \frac{T_{cp,(i-1)}}{n_i}, \tag{6.1}$$

where Δf_i and $T_{cp,(i)}$ denote the subcarrier spacing and the cyclic-prefix duration of the ith numerology and $n_i \in \mathbb{N}$ is a scaling factor. The duration of the OFDM symbol is the inverse of the subcarrier spacing. With this scaling approach, the sampling clock rates of different OFDM numerologies relate to each other via the scaling factors $\{n_i\}$, which simplifies the implementation. The 3GPP has adopted this scaling approach, i.e., the NR OFDM numerologies are derived from a baseline OFDM numerology (which is same as LTE numerology) via the scaling. In principle, the scaling factors $\{n_i\}$ could be selected independently of each other, however, it is desirable that the scaling factors follow a certain relationship to allow an efficient TDD based operation, which we discuss next.

For NR, the number of OFDM symbols per slot is equal for all numerologies, at-least up to the 120 kHz subcarrier spacing specified in 3GPP NR Release 15. Maintaining an equal number of OFDM symbols per slot for different numerologies simplifies scheduling and reference signal design. With the number of OFDM symbols per slot equal for all numerologies, the slot duration shrinks with the increase in the subcarrier spacing. This enables shorter latencies for wider subcarrier numerologies (to be used in high frequency small cell deployments where some of the low-latency applications are envisioned). Considering the equal numbers of OFDM symbols per slot for all numerologies, the following relationship holds for the respective slot durations between different numerologies:

$$T_{slot,(i)} = \frac{T_{slot,(i-1)}}{n_i} = \frac{T_{slot,(i-2)}}{n_i n_{i-1}} = \cdots = \frac{T_{slot,(1)}}{\prod_{k=1}^{i} n_k},$$

where $T_{slot,(i)}$ denotes the slot duration of the ith numerology. For adjacent TDD networks that are using different OFDM numerologies, it is desirable that an integer number of slots from one OFDM numerology fits into a slot of the other OFDM numerology to enable time-aligned downlink and uplink transmission periods. If the slot durations of different numerologies do not fulfill the above condition, then two neighboring TDD networks would require a guard time in the frame structure to enable synchronous operation, which will not be an efficient resource utilization. Therefore, the scaling factors are chosen such that a subcarrier spacing is integer divisible by all smaller subcarrier spacings, i.e.,

$$\Delta f_i = 2^{L_{(i)}} \Delta f_1, \qquad \forall i \in \{1, 2, ..., M\}, \tag{6.2}$$

where $L_{(i)} \in \mathbb{Z}$, M is the number of OFDM numerologies, and Δf_1 is subcarrier spacing of the base numerology. With this in mind, the 3GPP has specified the scaling factor as $n_i = 2^L$ in (6.1), where L is an integer.

6.3 OFDM NUMEROLOGY IMPLEMENTATION

The NR waveform is scalable—the subcarrier spacing of OFDM can be chosen according to 15×2^n kHz, where the integer-valued n is a design parameter and can be optimized for different scenarios. The 3GPP has agreed that NR should allow subcarrier spacing ranging from at least 3.75 kHz ($n = -2$) to 480 kHz ($n = 5$). A lower subcarrier spacing than 15 kHz (and a correspondingly longer cyclic prefix) is beneficial to support multicast-broadcast single-frequency network (MBSFN) transmission. For example, $n = -2$ results in a subcarrier spacing of 3.75 kHz, which is in the same range as the subcarrier spacings used in various digital broadcast standards, such as DVB, as well as being in line with some modes of NB-IoT. Hence, $n = -2$ is an option in the set of scaling factors to be considered. Choosing the value of n is not straightforward. It depends on various factors including type of deployments, service requirements, hardware impairments, mobility, performance, and implementation complexity. In the following, we provide a comprehensive discussion on these factors involved in selecting n for the NR waveform.

6.3.1 PHASE NOISE

Typically, phase noise increases with frequency of the local oscillator. It can be a major hardware impairment for NR deployments in high carrier frequencies, for example in the millimeter-wave band. Multicarrier waveforms are in general sensitive to phase noise. In an OFDM system, phase noise produces two types of degradations: a common phase error (CPE) and an intercarrier interference (ICI). We will discuss these in the following.

Consider a received baseband signal subject to phase noise $r[n] = x[n]e^{j\phi[n]}$, where $\phi[n]$ is a random process. Typically, in Phase-Locked-Loop (PLL)-based oscillators, $\phi[n]$ is a Wide-Sense Stationary (WSS) random process and $|\phi[n]| \ll 1$ [11], which leads to the following approximation:

$$r[n] = x[n]e^{j\phi[n]} \approx x[n]\,(1 + j\phi\,[n])\,. \tag{6.3}$$

Under this approximation, the demodulation of subcarrier $l \in \{1, 2, \ldots, N\}$ in an OFDM system with total N subcarriers is given by

$$\begin{aligned} R_l &= \frac{1}{N}\sum_{n=0}^{N-1} r[n]\mathrm{e}^{-j2\pi\frac{l}{N}n} \\ &\overset{(a)}{=} \frac{1}{N}\sum_{n=0}^{N-1}\sum_{i=0}^{N-1} X_i \mathrm{e}^{j2\pi\frac{i}{N}n}\mathrm{e}^{-j2\pi\frac{l}{N}n}(1 + j\phi[n]) \\ &= X_l + j\frac{X_l}{N}\sum_{n=0}^{N-1}\phi[n] + j\sum_{n=0}^{N-1}\sum_{i=0,i\neq l}^{N-1} X_i \mathrm{e}^{j2\pi\frac{i-l}{N}n}\phi[n] \end{aligned}$$

$$\stackrel{(b)}{=} X_l\,(1+\varphi) + N_l^{ICI}, \tag{6.4}$$

where (a) follows from $x[n] = \sum_{i=0}^{N-1} X_i \mathrm{e}^{j2\pi \frac{i}{N} n}$ and (6.3) and (b) follows by defining $\varphi := j\sum_{n=0}^{N-1} \phi[n]$ and $N_l^{ICI} := jX_l \sum_{n=0}^{N-1} \sum_{i=1, i\neq l}^{N} X_i \mathrm{e}^{j2\pi \frac{i-l}{N} n} \phi[n]$. According to (6.4), the transmitted symbol X_l is multiplied by the term $(1+\varphi)$. This is known as the common phase error (CPE) as it causes identical phase rotations in all subcarriers. The additive noise term N_l^{ICI} refers to the intercarrier interference, which is different for different subcarriers.

The CPE is an identical phase rotation in all subcarriers within an OFDM symbol, therefore it can easily be compensated for using pilot subcarriers (reference signals). (See Section 2.5 for an introduction to different reference signals specified for NR.) For a fast varying channel, the CPE can be compensated as part of a channel estimation process. However, for a slowly varying channel, the CPE needs to be tracked and compensated for more frequently. The 3GPP has introduced the PT-RS in NR mainly for the CPE compensation. In addition, the DM-RS whenever present, can also be used for the CPE compensation. Both the DM-RS and the PT-RS are discussed in Section 2.5.

The ICI is an additive noise (not always Gaussian) and often hard to compensate for, depending on how fast the phase noise variations are. Although the PT-RS can also be utilized for the ICI compensation, it typically requires denser pilot allocation which can degrade the system throughput.[7] An alternative is to chose the waveform numerology (the subcarrier spacing) such that there is sufficient robustness to the ICI. For a typical oscillator, the impact of the ICI decreases as the subcarrier spacing of the signal increases, as discussed in Section 5.5.5. Therefore, an OFDM system can be made robust against the ICI by choosing a larger subcarrier spacing.[8] A too low choice of the subcarrier spacing either puts strict requirements on the local oscillator or phase noise puts an upper limit on the achievable performance under the ICI. In Section 5.5.5, we have quantified the signal-to-interference ratio (SIR) due to the ICI in an OFDM system (cf. (5.24)). Assuming a perfect CPE compensation, the achievable signal-to-interference ratio (SIR) over the demodulated subcarrier l in an OFDM symbol (subject to phase noise) is given by

$$\mathrm{SIR}_l = \frac{1}{\left(\int_{-0.5}^{+0.5} S_\phi(\nu)\, W_l(\nu)\, d\nu\right)}, \tag{6.5}$$

where

$$W_l(\nu) := \sum_{i \in I_{ICI}} \frac{1}{N^2} \left| \frac{\sin\left(\pi\left(\nu - \frac{i-l}{N}\right) N\right)}{\sin\left(\pi\left(\nu - \frac{i-l}{N}\right)\right)} \right|^2. \tag{6.6}$$

In Fig. 6.4 we show the achievable SIRs for different subcarrier spacings based on a PLL based phase-noise model presented in Section 4.2.3. This phase-noise model was developed in mmMAGIC

[7] The density of the PT-RS is configurable in both time and frequency domains.

[8] It is noteworthy that the value of the CPE is constant only within one OFDM symbol. The value of CPE varies from one OFDM symbol to another OFDM symbol and its variance can increase with the subcarrier spacing (in contrast to the ICI). Therefore, an OFDM system becomes more robust against phase noise by employing the larger subcarrier spacings only if the CPE compensation is in place, which is the case for NR.

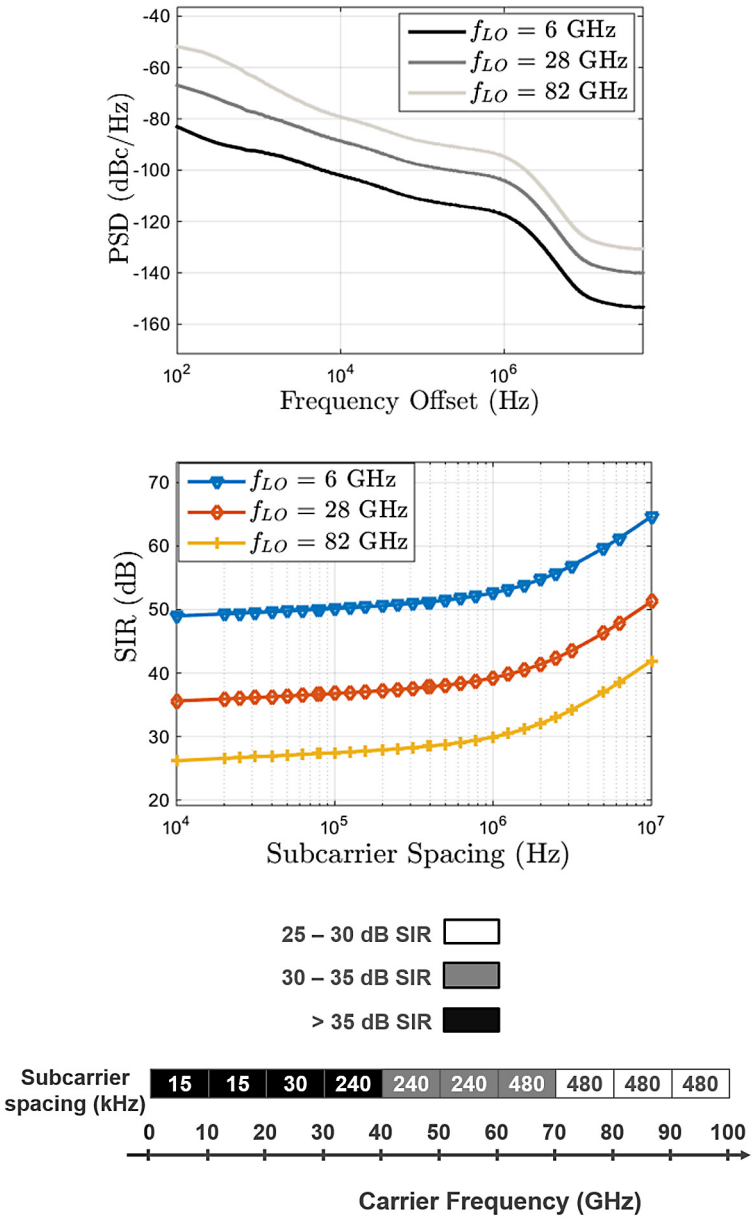

FIGURE 6.4

Achievable Signal-to-Interference Ratio (SIR) in a 100 MHz OFDM system subject to phase-noise for different subcarrier spacings. The CPE is assumed to be perfectly compensated for. (The phase-noise model is developed within mmMAGIC project.)

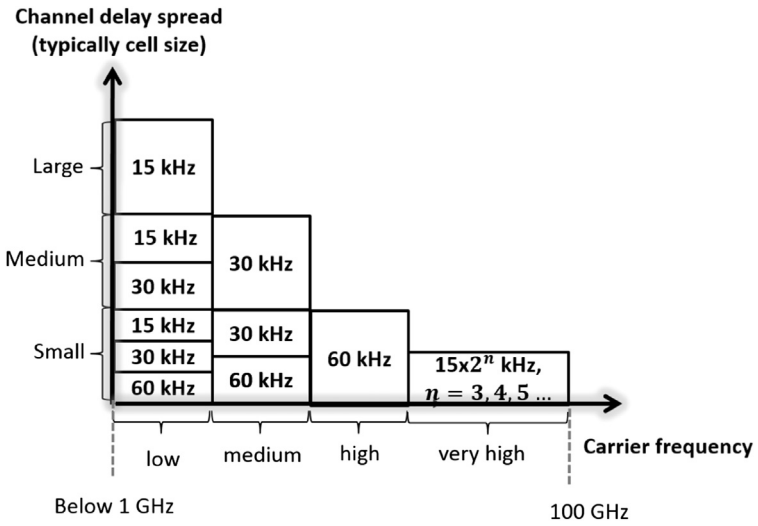

FIGURE 6.5

The NR numerology for wide range of frequencies and deployment types.

project[9] [7]. The phase-noise power spectral densities and the corresponding achievable SIRs are shown for three oscillator frequencies (6 GHz, 28 GHz, and 82 GHz). Towards the bottom of Fig. 6.4, we further specify which subcarrier spacings achieve the SIR values above 25 dB for carrier frequencies up to 100 GHz (assuming the mmMAGIC phase-noise model).

6.3.2 CELL SIZE, SERVICE LATENCY, AND MOBILITY

In an OFDM system, the cyclic prefix is chosen larger than the channel delay spread to avoid inter-symbol interference and complex equalization. This means that for a given cyclic-prefix overhead, the channel delay spread sets a lower limit on the subcarrier spacing. Typically, the delay spread reduces with cell size and so does the required cyclic-prefix duration, meaning that wider subcarrier spacings (having shorter cyclic prefix) are more suitable for deployments with smaller cell size. This goes hand-in-hand with the fact that smaller cell sizes are envisioned at higher carrier frequencies due to harsh propagation characteristics and wider subcarrier spacing that make the system robust to phase noise (which increases with oscillator frequency). Numerologies with wider subcarrier spacings are also suitable for supporting low-latency services, since the transmission slot duration (as defined in Table 6.2) is inversely proportional to the subcarrier spacing. This implies that low latencies can be achieved in small cells using a numerology with wider subcarrier spacing. Fig. 6.5 and Fig. 6.6 illustrate the relationships between cell size, carrier frequency, and achievable latency for NR.

[9] mmMAGIC was an EU project (funded by the H2020 program) that developed radio interface concepts and solutions for above 6 GHz mobile radio communications. https://5g-mmmagic.eu/.

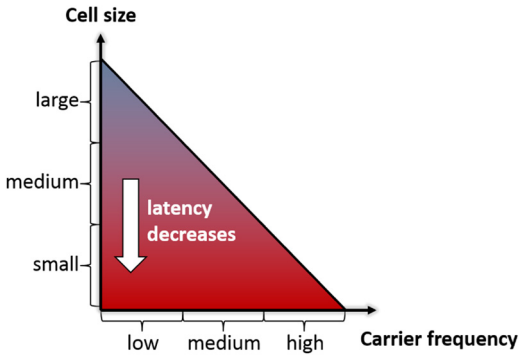

FIGURE 6.6

The relationship of achievable latency, carrier frequency, and deployment type for NR.

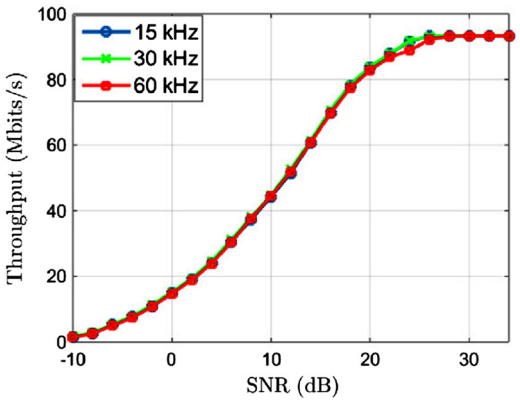

FIGURE 6.7

TDL-A channel model with 300 ns RMS delay spread.

Low latency can also be achieved in larger cells using wider subcarrier spacing, however, this can cost loss in performance either in terms of reliability or throughput. To understand this, we evaluate achievable throughput for three numerologies (15 kHz, 30 kHz, and 60 kHz) assuming the 7% CP overhead (as specified in 3GPP) subject to the Tapped Delay Line-A (TDL-A) channel model [14] with two different delay spread values (300 ns and 1000 ns). The results are shown in Fig. 6.7 and Fig. 6.8, respectively. In these simulations, we have assumed 1 ms TTI (i.e., 14 OFDM symbols for 15 kHz numerology, 28 OFDM symbols for 30 kHz numerology, and 56 OFDM symbols for 60 kHz numerology). Furthermore, we have considered link adaptation, with 64 QAM as the highest modulation order. In Fig. 6.7, we observe that all numerologies perform similarly, meaning that one can reduce the CP duration to four times smaller than what we have in LTE or one can also enable wider subcarriers to support latency critical services. Fig. 6.8 shows that the 60 kHz numerology should not

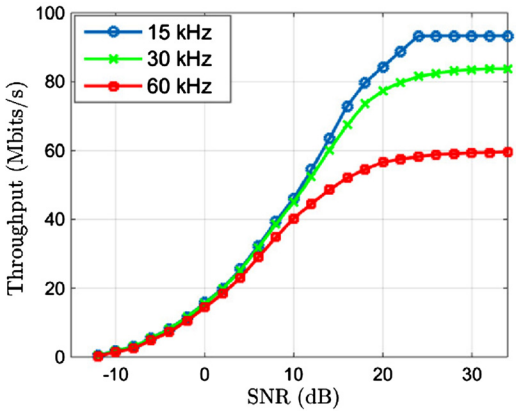

FIGURE 6.8

TDL-A channel model with 1000 ns RMS delay spread.

be used in delay spread intensive environments. One can use 60 kHz subcarrier spacing in the delay spread intensive environments with an extended cyclic prefix to support very low latency machine-type communications. However, extending the CP duration means higher overhead, and hence reduced throughput. The 3GPP has included an option of extended CP with 25% overhead for 60 kHz subcarrier spacing in NR Release 15. It is, however, important to note that the mini-slot based transmission is an alternative method to achieve very low latency without increasing the CP overhead (as discussed in Section 6.2).

In an OFDM system, the relative mobility between a user and an access node causes intercarrier interference (channel time variations or the Doppler effect leads to loss of subcarrier orthogonality). On the one hand, the Doppler effect increases with increasing carrier frequency for a given mobile scenario. On the other hand, the cell size is expected to reduce at higher carrier frequencies for 5G deployments, which implies UEs with low mobility (speeds) relative to the base station (access node). If small cells are realized at high carrier frequencies, mobility may not be a limiting factor in choosing numerology. However, for high-speed scenarios (e.g., V2V) in the millimeter-wave band, the Doppler effect can set a lower limit on the choice of the subcarrier spacings.

6.3.3 MULTIPLEXING SERVICES

Multiple services with different requirements (eMBB, mMTC, URLLC) can be efficiently supported on the same carrier by either using mini-slots or by multiplexing different OFDM numerologies in the frequency domain. For example, the mini-slot can be used to support a URLLC service within the regular slot that supports an eMBB service. Alternatively, a wideband subcarrier numerology and a narrowband subcarrier numerology can be multiplexed to support URLLC and MBB services, respectively. Fig. 6.9 illustrates these two options. Mini-slot is the preferred option due to the following drawbacks of the mixed numerology.

In an OFDM system with two (or more) different numerologies (subcarrier bandwidth and/or cyclic-prefix length) multiplexed in the frequency domain, only subcarriers within a numerology are

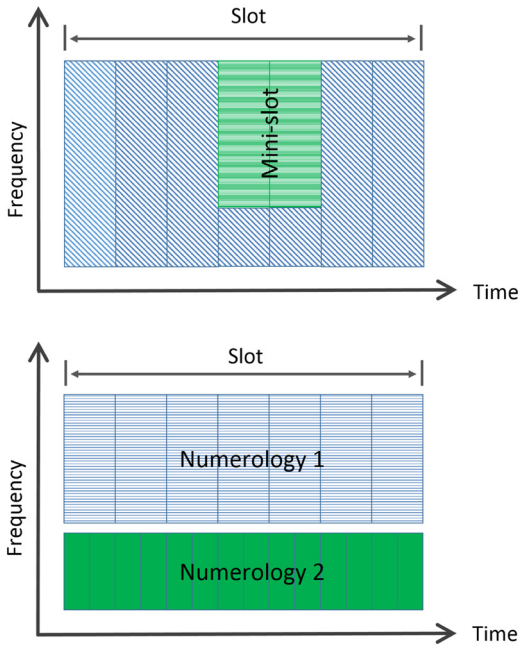

FIGURE 6.9

The mini-slot and the mixed numerology are two alternative tools for multiplexing services with different requirements on the same carrier.

mutually orthogonal. The subcarriers from one numerology interfere with the subcarriers of the other numerology, since energy leaks outside the subcarrier bandwidth and is picked up by subcarrier filters of the other numerology, as illustrated in Fig. 6.10. To reduce the internumerology interference, the transmit spectrum of each numerology must be better confined and a guard band is typically required. Moreover, an extended CP may be required with wider subcarrier spacings, depending on the channel delay spread.

6.3.4 SPECTRAL CONFINEMENT

Spectral confinement is important to reduce out-of-band (OOB) emissions. The 3GPP specifies the OOB emission requirements[10] for both base stations and devices. The better the spectrum roll-off of the signal, the easier it is to fulfill these requirements. The spectrum of the OFDM signal decays rather slowly (see Chapter 5) and the specified OOB emission requirements cannot be fulfilled without inserting guardband[11] and performing additional filtering/windowing operations. The spectrum roll-off of the OFDM signal becomes steeper as its subcarrier spacing reduces. As an example, PSDs of two

[10]The OOB emission requirements are specified in terms of spectrum emission mask and adjacent channel leakage ratio.
[11]LTE occupies 90% of the channel bandwidth. In 3GPP Release 15, the spectrum utilization for NR is above 94%.

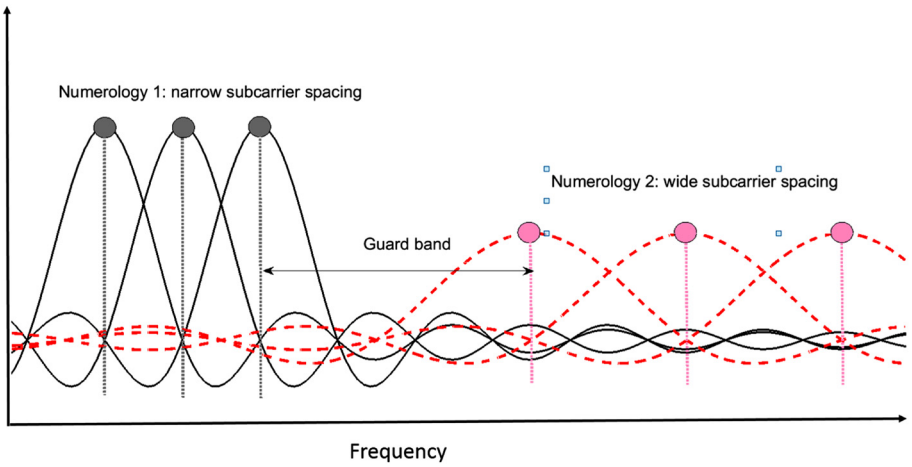

FIGURE 6.10

An illustration of the internumerology interference.

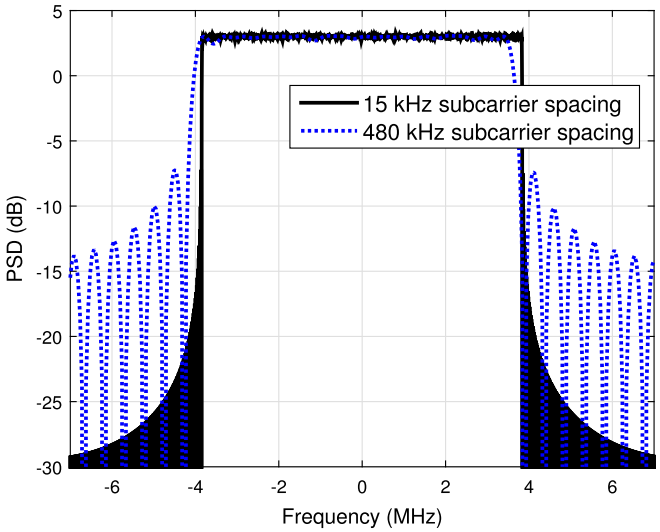

FIGURE 6.11

Comparison of OOB emissions of OFDM signals with 15 kHz and 480 kHz subcarrier spacing.

equal bandwidth OFDM signals with subcarrier spacing of 15 kHz and 480 kHz are shown in Fig. 6.11. This speaks in favor of avoiding too large subcarrier spacings in NR.

Spectral confinement is also important for reducing the internumerology interference. This can be understood with the help of Fig. 6.12 that shows two subbands with different numerologies multiplexed

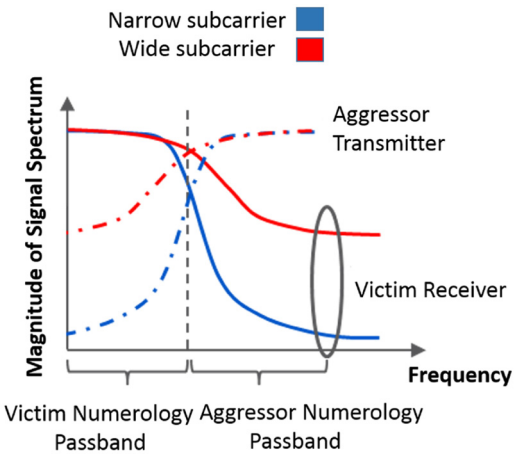

FIGURE 6.12

Both the transmitter and the receiver filtering functionality must be improved to reduce the internumerology interference efficiently.

in the frequency domain. The aggressor numerology (dash-dotted lines) must apply a spectrum emission confinement technique to reduce the energy transmitted in the passband of the victim numerology (blue[12] dash-dotted line). However, the emission control alone is not sufficient, since a victim receiver without steeper roll-off (solid red[13] curve) picks up high interference from the passband of the aggressor numerology. Only if the victim receiver (solid blue curve) and the aggressor transmitter (dashed blue curve) have improved filter functions, the internumerology interference is efficiently reduced.

Windowing and filtering are well-known techniques to confine spectrum of the OFDM signal [1,12]. Windowing has lower implementation complexity than filtering. A low complexity windowing operation can significantly improve spectrum confinement at the expense of consuming a small portion of the CP [20]. In Fig. 6.13, we compare throughput performance of OFDM without mixed numerology and W-OFDM[14] in a mixed numerology scenario where a 15 kHz numerology is multiplexed with a 60 kHz numerology. We assume that the 15 kHz numerology has 6 PRBs[15] and the 60 kHz numerology has 21 PRBs. Fig. 6.13 shows the throughput achieved by the 15 KHz numerology (i.e., considering the 60 kHz numerology as the aggressor and the 15 kHz numerology as the victim). We have used the TDL-A channel model with 1000 ns RMS delay spread (which is larger than what is typically experienced in most scenarios) and up to 64-QAM modulation for link adaptation. The two numerology subbands are separated by a guard band of 120 kHz (i.e., eight 15 kHz subcarriers). This result demonstrates that the throughput performance of W-OFDM with interference from the aggressor is close to CP-OFDM without any interference from the aggressor, even under extreme conditions with very large channel delay

[12] Dark gray in print version.
[13] Light gray in print version.
[14] W-OFDM is introduced in Section 5.1.2.2.
[15] A physical resource block contains 12 subcarriers in NR, like LTE.

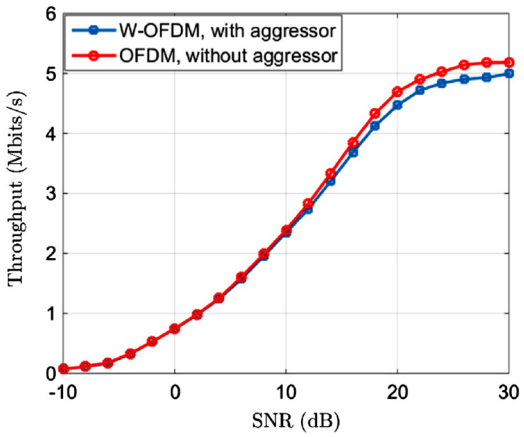

FIGURE 6.13

Comparison of W-OFDM with interference from the aggressor numerology and OFDM without interference from the aggressor numerology on TDL-A channel with 1000 ns RMS delay spread. The victim numerology is narrowband (15 kHz subcarrier spacing with 6 PRBs), the aggressor numerology is wideband (60 kHz subcarrier with 21 PRBs), and the guard band is 120 kHz.

spread, narrowband victim numerology, and wideband aggressor numerology. Hence, windowing on top of CP-OFDM is a low complexity viable technique to multiplex multiple numerologies in NR.

6.3.5 GUARD BAND CONSIDERATIONS

Guard tones can be inserted between numerologies to reduce internumerology interference and/or relax the degree of required spectrum confinement. Adding guard tones slightly increases the overhead. In a 20 MHz system with 1200 subcarriers, one guard tone corresponds to less than 0.1% overhead. It may not be worth the effort to reduce the guard band to an absolute minimum, since it increases the requirements on the spectrum confinement technique (both at transmitter and receiver) and also complicates other system design aspects, as discussed in the following.

Consider Fig. 6.14, where one narrowband subcarrier is inserted as a guard tone between numerology 1 (15 kHz subcarrier spacing) and numerology 2 (60 kHz subcarrier spacing). A physical resource block in NR contains 12 subcarriers for all numerologies. If the scheduling is done as indicated for numerology 2, then the subcarriers of numerology 2 are not on the 60 kHz resource grid (the first subcarrier of the blue (light gray in print version) resource block is on narrow subcarrier 41, which corresponds to the wide subcarrier 10.25, i.e., there is a fractional subcarrier shift).

To avoid such fractional subcarrier shift, subcarrier frequencies in each numerology should coincide with the natural grid of the numerology $n \times \Delta f$, with Δf the subcarrier spacing of the numerology. However, even with this requirement the wide resource blocks (numerology 2) are still not on their natural grid if compared to cell 2; see Fig. 6.15. Such a misaligned resource grid implies that all users of numerology 2 would have to be dynamically informed as regards this offset (since this offset depends on the scheduling decision). In another cell, a different offset may be present or another cell

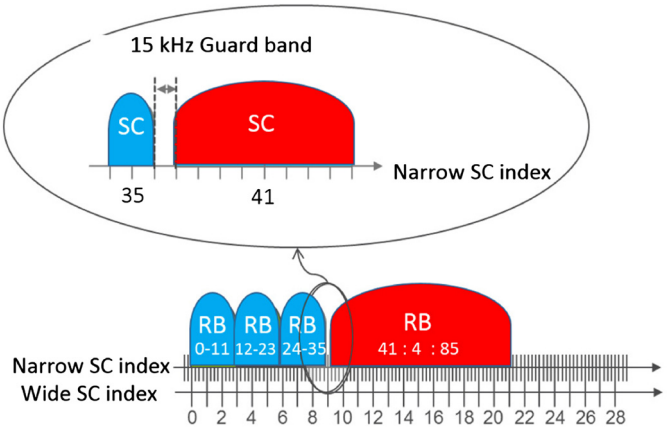

FIGURE 6.14

One narrowband subcarrier (SC) is inserted as a guard between numerology 1 (15 kHz) and numerology 2 (60 kHz). The first subcarrier of numerology 2 is located at 41 × 15 kHz, which corresponds to subcarrier 10.25 in a 60 kHz subcarrier grid.

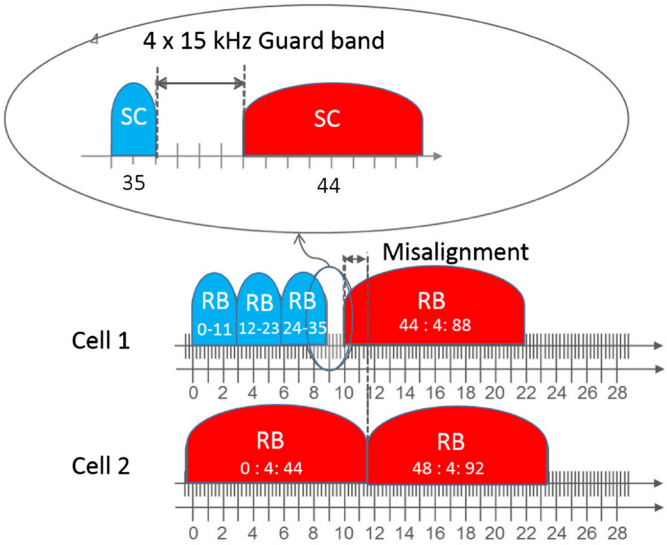

FIGURE 6.15

Four narrowband subcarriers are inserted as a guard between numerology 1 (15 kHz) and numerology 2 (60 kHz). The subcarriers of numerology 2 are located on its natural resource grid. However, numerology 2 resource blocks are still misaligned across cells.

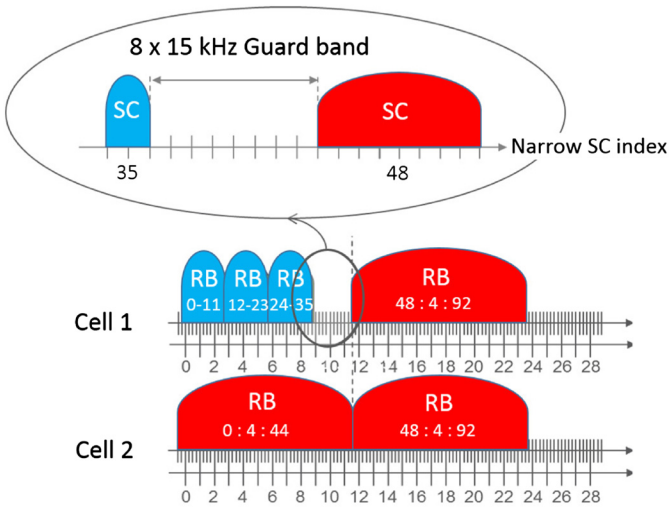

FIGURE 6.16

Eight narrowband subcarriers are inserted as guard between numerology 1 (15 kHz) and numerology 2 (60 kHz). The subcarriers of numerology 2 are located at its natural resource grid and numerology 2 resource blocks are aligned across cells.

may only operate with numerology 2 (as shown in Fig. 6.15). The resource blocks in different cells would not be aligned making intercell interference coordination (ICIC),[16] creation of orthogonal reference signals across cells, and interference prediction across cells more difficult. Alternatively, the first red (dark gray in print version) resource block in cell 1 in Fig. 6.15 could be a fractional resource block (corresponding to the bandwidth marked by misalignment). Special definitions of the reference signals and rate matching would be required for all possible fractional resource blocks. For the fractional resource block in cell 1 and the overlapping resource block in cell 2, the same disadvantages exist.

The cleanest solution is to limit the location of the resource blocks to their natural resource grids. For example, as shown in Fig. 6.16, numerology 1 (15 kHz) resource blocks always start at a frequency of $n \times 12 \times 15$ kHz and numerology 2 (60 kHz) resource blocks start at a frequency of $n \times 12 \times 60$ kHz. This simplifies the ICIC, makes the interference predication across cells easier, and enables orthogonal reference signals of the same numerology across cells. For the (15 kHz, 60 kHz) numerology combination, the resulting guard band is eight narrowband (15 kHz) subcarriers. In a 20 MHz system with around 1200 narrowband subcarriers, the spectral loss due to this guardband is less than 1%.

[16]The ICIC refers to the coordination between neighboring base stations to avoid severe interference situations. The overall system efficiency and user experience can be significantly improved with the ICIC, especially in heterogeneous network deployments with overlapping layers of base stations with large differences in the downlink transmission power.

6.3.6 IMPLEMENTATION ASPECTS

OFDM is implemented in baseband via the fast Fourier transform (FFT) operation (see Fig. 5.7). The FFT/IFFT size should be selected considering the subcarrier spacing, the channel bandwidth, and the affordable computational complexity. The asymptotic complexity of an N-point FFT operation is $\mathcal{O}(N \log N)$. For a given subcarrier spacing, the FFT size determines the maximum channel bandwidth (without carrier aggregation). The maximum channel bandwidth in LTE is 20 MHz, with 2048 FFT size, 30.72 MHz sampling rate, and 1200 is the number of active carriers (100 PRBs). In 3GPP NR Release 15, the maximum number of active subcarriers is 3300 and the largest currently defined channel bandwidth occupies 3276 subcarriers. This can be implemented using an FFT size of 4096. Note that a smaller FFT size may be used if the number of active subcarriers is less.

6.4 IMPROVING POWER EFFICIENCY OF NR WAVEFORM

A major drawback of OFDM waveform is its high PAPR. A high PAPR in the OFDM system causes the power amplifier to operate in a nonlinear region, which contributes to a spectral growth in the form of intermodulation between subcarriers and out-of-band emissions, as described in Section 4.1. Therefore, to keep the nonlinear effects within certain limits, the power back-off is commonly used in the power amplifier, which reduces the coverage. Another possibility is to increase the linear region of the power amplifier, which in turn results in larger amplifiers and hence, higher power consumption. A very common solution is to deploy DPD algorithms to cancel out the nonlinear distortion from the amplifier. This, however, is a high complexity solution, in particular for large antenna arrays.

The power efficiency of the waveform can be very important in the uplink and the sidelink, for coverage limited UEs. A high PAPR (with a high power back-off requirement) mainly affects the highest output transmission power level for the UE. Hence, a low PAPR is more relevant to the coverage-limited UEs. In LTE, the downlink uses OFDM, while the uplink and the sidelink use DFTS-OFDM due to its lower PAPR than OFDM. (See Section 5.2 for an introduction to DFTS-OFDM.) For NR, the 3GPP has specified DFTS-OFDM as an optional[17] waveform for the uplink, however, without spatial multiplexing (MIMO). A MIMO DFTS-OFDM transceiver has a significantly higher implementation complexity than OFDM and worse performance than OFDM. Furthermore, in the coverage limited scenarios spatial multiplexing is often not useful. Typically, UEs at the cell edge use only a small number of resource blocks (i.e., narrow bandwidth allocation) for transmission with low spectral efficiencies (low code rate and low order modulation formats, e.g., QPSK). Due to these reasons, NR supports DFTS-OFDM only for a single stream transmission in the uplink.

When a UE is in good cell coverage and has a wide bandwidth allocation, a high PAPR is often not critical. In this scenario, OFDM is the natural choice. Using OFDM instead of DFTS-OFDM in the uplink (and also in the sidelink) has several advantages:

- MIMO transmission is one of the key features of NR and it is expected that even uplink MIMO will be widely adopted for the enhanced mobile broadband usage (see Chapter 7). With MIMO

[17] In 3GPP NR Release 15, DFTS-OFDM is optional in the uplink and it is up to the base station to select which waveform (OFDM or DFTS-OFDM) should be used in the uplink. This implies that an NR capable UE need to implement both waveforms and a gNB (or base station) can choose to implement only OFDM.

transmission, OFDM is known to provide a significant superior link performance compared to DFTS-OFDM [8].
- DFTS-OFDM requires an additional DFT precoder in the transmitter and an extra IDFT decoder and equalizer in the receiver which increases the baseband complexity, significantly with the MIMO transmissions.
- OFDM is more flexible than DFTS-OFDM in terms of scheduling users' data, control signals, and reference signals, resulting in an enhanced system capacity.
- Having the same transmission scheme in both uplink and downlink makes the whole system design symmetric. A single waveform (i.e., OFDM) for all link types (uplink, downlink, sidelink, backhaul link) simplifies the design by avoiding the need for separate baseband implementations for different waveforms.

Although using OFDM in the uplink comes with major advantages, yet it suffers from the problem of the high PAPR which should be addressed if it is to be employed in all scenarios. There exist several PAPR reduction techniques for OFDM with their pros and cons [10]. While choosing an appropriate PAPR reduction technique, several factors need attention. For example, the PAPR reduction capability, implementation complexity, transparency between the transmitter and the receiver sides, and link performance degradation. Some of the techniques require implementation of multiple FFTs and/or transmission of side information to the receiver, which may be either undesirable or not possible.[18] In the following, we provide a brief overview of some well-known PAPR reduction schemes based on [10]. Broadly speaking, one can divide the PAPR reduction methods into two groups: i) techniques with distortion, and ii) distortion-less techniques.

6.4.1 TECHNIQUES WITH DISTORTION

The following schemes distort the OFDM signal while reducing its PAPR:

- **Clipping** The most simple and widely used technique is to limit the signal envelope to a predefined threshold by means of an amplitude clipper. The amplitude clipping function is given by

$$f\left(x[n]\right) = \left\{ \begin{array}{c} x[n], \quad |x[n]| \leq A_{max}, \\ A_{max}\exp(j\phi(x[n])), \quad |x[n]| > A_{max}, \end{array} \right\} \tag{6.7}$$

  where A_{max} is the amplitude threshold and $\phi(x[n])$ is the phase of $x[n]$. Clipping is a nonlinear transformation of the signal. It causes both in-band and out-of-band distortions. The out-of-band distortion can be reduced by performing filtering after clipping. However, the filtering operation may increase the signal amplitude above the clipping threshold. To address this issue, repeated clipping and filtering operations may be employed at the cost of increased implementation complexity. The in-band distortion cannot be improved by filtering and therefore degrades the BER performance and the spectral efficiency.
- **Companding** Companding refers to a nonlinear transformation of a signal in which lower signal amplitude levels are increased and peak signal amplitudes remain unchanged. The average signal

[18] In 3GPP NR Release 15, any operation performed on CP-OFDM at the transmitter side has to be receiver agnostic.

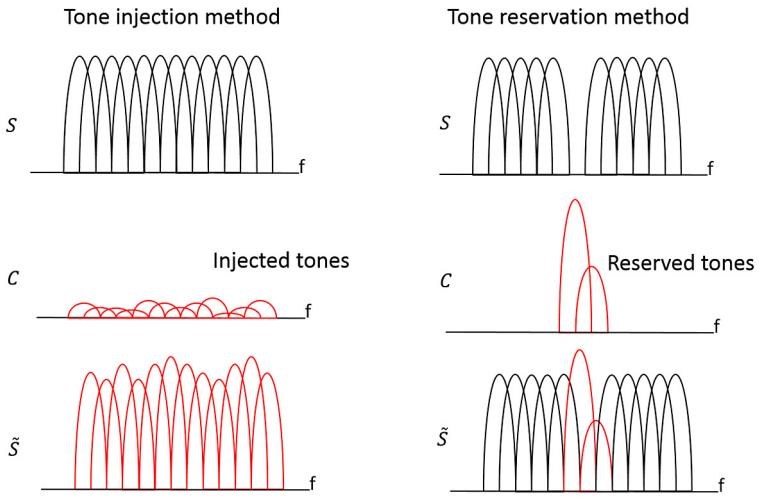

FIGURE 6.17

An illustration of Tone Injection (TI) and Tone Reservation (TR) methods.

power increases after the companding operation, which reduces PAPR. Several companding transformations exist in the literature, for example, exponential companding and polynomial companding are widely used. Companding is an invertible transformation since the companding function is a monotonically increasing function, unlike clipping. This means that a companded signal can be recovered at the receiver by applying an inverse transformation. Both the clipping and the companding methods have low implementation complexity, however, they give rise to relatively high spectral emissions.

- **Tone Injection (TI)** Tone injection refers to superimposing additional subcarriers with optimized amplitude and phases on the information bearing data subcarriers. An illustration is shown in Fig. 6.17 for the injection of the additional tones C into the data subcarriers S to get a PAPR reduced signal $\tilde{S} = S + C$. This is equivalent to expanding the constellation size of the signal, i.e., each point in the original constellation can be mapped in different points in the expanded constellation. As each data symbol can be mapped to one of the several equivalent constellation points, the transmitter can use this degree of freedom to reduce the PAPR. In this case, the receiver needs to know how to map the redundant constellations to the original constellation.
- **Active Constellation Extension (ACE)** ACE is similar to TI, but with the difference that in ACE only outer constellation points are dynamically extended away from the original constellation. Constellation extension gives additional degrees of freedom to reduce the PAPR by optimizing the constellation points. By extending the outer constellation, the spacing between constellation points also increases, which improves BER performance. A drawback of ACE is the increase in transmit power. The usefulness of ACE is restricted to the modulation schemes with large constellation size.

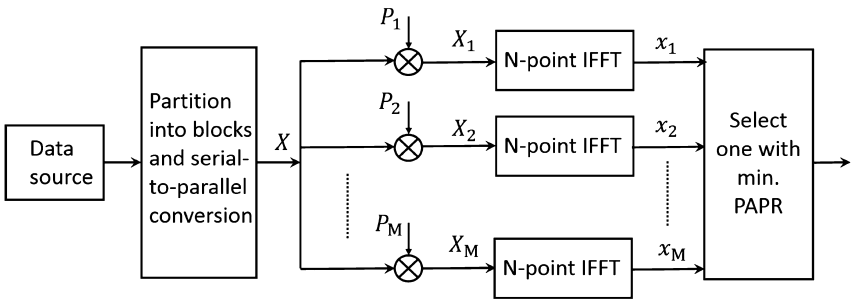

FIGURE 6.18

A schematic of Selective Mapping (SLM) method.

6.4.2 DISTORTION-LESS TECHNIQUES

The following PAPR reduction schemes do not introduce distortion:

- **Tone Reservation (TR)** In this technique, a set of subcarriers within an OFDM symbol are reserved solely for the PAPR reduction. These reserved subcarriers do not carry any data; they are modulated such that the summation of all subcarriers (the data subcarrier and the reserved subcarriers) generate a signal with a low PAPR. In Fig. 6.17, an illustration is given for the superposition of the reserved tones C with the data subcarriers S to get a PAPR reduced signal $\tilde{S} = S + C$. The procedure of finding and optimizing the reserved tones is typically of moderate complexity. The effectiveness of this method depends on the number of reserved tones.
- **Selective Mapping (SLM)** In this method, a number of data blocks carrying same information are generated and the data block that has lowest PAPR is selected for transmission, as shown in Fig. 6.18. Different data blocks are generated by multiplying modulated symbols with different phase vectors before IFFT. The information as regards phase vectors has to be transmitted to the receiver. Therefore, this scheme is not transparent to the receiver and there is a loss of spectral efficiency due to the transmission of side information. The PAPR reduction ability of this method is directly related to the implementation complexity; the larger the set of phase vectors and the number of IFFTs, the higher will be the PAPR reduction capability.
- **Partial Transmit Sequence (PTS)** In this method, the input data block is divided into a set of disjoint subblocks. Each subblock is padded with zeros, IFFT operation is performed on each subblock, which is then multiplied with a phase vector, as shown in Fig. 6.19. The subblocks are then combined such that PAPR of the time-domain OFDM signal is minimized.
- **Suitable Coding** The idea is to select the codewords that reduce the PAPR of the transmitted signal. Peak power is achieved in the OFDM signal when N subcarriers with same phase values are superimposed. The peak power is N times the average power. However, not all codewords result in a high PAPR. The codewords can be selected such that likelihood of occurrence of the same phase for N subcarriers can be minimized. Various coding methods have been shown effective for reducing the PAPR. A drawback of the coding-based PAPR reduction methods is the potential loss in the coding rate (i.e., lower spectral efficiency).

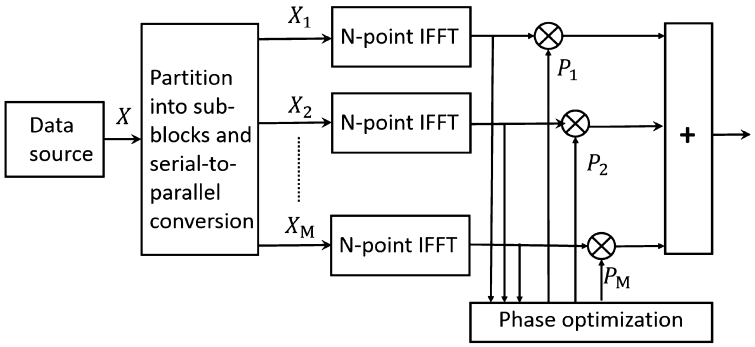

FIGURE 6.19

A schematic of Partial Transmit Sequence (PTS) method.

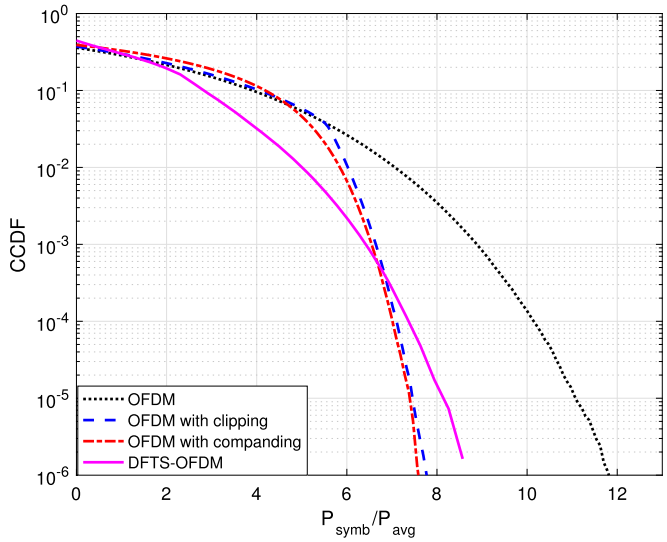

FIGURE 6.20

CCDF of PAPR (P_{symb}/P_{avg}).

Next, we look at the effectiveness of two low complexity PAPR reduction techniques—the clipping and the companding methods. We assume the following OFDM parameters: 2048 FFT size, 60 kHz subcarrier spacing, and 16 QAM modulation. The exponential companding degree is set to 1 and the clipping ratio (i.e., the ratio of the amplitude threshold to the square root of the average power of the signal) of the amplitude clipping scheme is set to 1.7, in order to have similar level of PAPR reduction with the two schemes. Fig. 6.20 shows the CCDF of the ratio of the instantaneous power of an OFDM symbol (P_{symb}) to the average power (P_{avg}) of the OFDM system with and without different PAPR

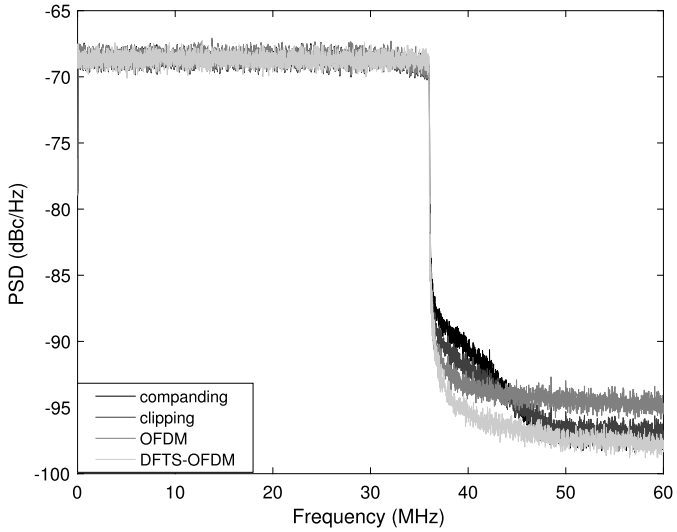

FIGURE 6.21

PSD of OFDM signals with and without different PAPR reduction schemes.

reduction schemes. For comparison, the PAPR performance of a DFTS-OFDM signal is also plotted in the same figure. The effectiveness of the clipping and exponential companding schemes in the OFDM system is clearly demonstrated. Fig. 6.21 shows the PSDs of the OFDM signals with and without the PAPR reduction schemes. For comparison, the PSD of the DFTS-OFDM signal is also included in the figure. We observe that there is some spectral regrowth when these PAPR reduction schemes are employed (which is one of the drawbacks). Nevertheless, we conclude that the high PAPR issue of OFDM can be addressed by implementation of a PAPR mitigation scheme which is not complex from the implementation point of view and achieves similar performance as DFTS-OFDM.

6.5 EFFECTS OF SYNCHRONIZATION ERRORS

In general, an OFDM system is robust to timing synchronization errors due to the presence of the cyclic prefix. However, it is sensitive to frequency synchronization errors due to its overlapping orthogonal narrowband subcarriers that can lose orthogonality when subject to frequency errors. In this section, we will briefly discuss the effects of timing and frequency synchronization errors in an OFDM system.

6.5.1 EFFECT OF TIMING OFFSET

Consider a discrete time OFDM signal with its mth OFDM symbol denoted as $x_m[n] = \sum_{i=0}^{N-1} X_{m,i} \times e^{j2\pi \frac{i}{N} n}$, having N subcarriers (generated by an N point IFFT) and N_{cp} cyclic-prefix samples. To

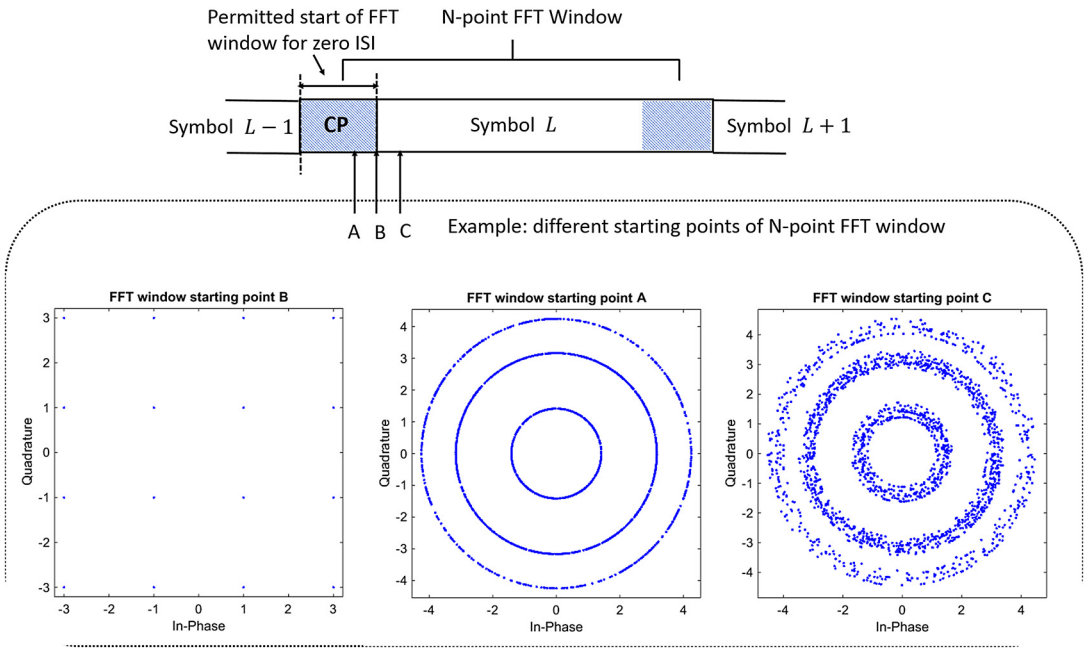

FIGURE 6.22

Effects of timing offset in an OFDM system.

demodulate this signal, an OFDM receiver must place an FFT window (perform an FFT operation) on N consecutive samples of each OFDM symbol. The ideal FFT window starting point is the first sample after the removal of the cyclic prefix, which leads to a perfect reconstruction of the transmitted modulation symbols. This is illustrated in Fig. 6.22 as the starting point B, along with the effects of starting an FFT window within the CP duration (the starting point A) and outside the CP duration, capturing portion of another symbol (the starting point C). For the starting point A (FFT window within the CP duration), the demodulated QAM symbols experience phase rotation (a frequency error). Mathematically, the demodulated subcarriers in this case are given by

$$\hat{X}_{m,k} = X_{m,k} \mathrm{e}^{\frac{-j2\pi n_o k}{N}}, \quad k = 1, 2, \ldots, N, \tag{6.8}$$

where n_o is the timing offset. According to (6.8), the kth subcarrier experiences a phase shift $\mathrm{e}^{\frac{-j2\pi n_o k}{N}}$. This phase shift (or the timing offset n_o) can be estimated (via pilot subcarriers) and easily compensated for in the frequency domain (post FFT). Hence, a timing offset of $1 \leq n_0 \leq N_{cp}$ is not problematic. In practice, when a signal is received over a multipath channel with maximum delay spread L, a timing offset of $1 \leq n_0 \leq N_{cp} - L$ is tolerable.

The timing offset become problematic when an FFT window captures samples of an adjacent OFDM symbol (i.e., the FFT window starts after the first OFDM sample in a CP removed symbol), illustrated by the starting point C in Fig. 6.22. In this case the demodulated subcarriers suffer from

intercarrier interference (ICI) and intersymbol interference (ISI). Mathematically, the kth demodulated subcarrier in the mth OFDM symbol subject to ICI and ISI (from $m+1$th OFDM symbol) due to the timing offset n_o is given by

$$R_{m,k} = X_{m,k}\left(1-\frac{n_o}{N}\right)\mathrm{e}^{\frac{j2\pi n_o k}{N}} + \underbrace{\frac{1}{N}\sum_{n=0}^{N-1-n_o}\sum_{\bar{k}=0;\bar{k}\neq k}^{N-1} X_{m,k}\mathrm{e}^{\frac{j2\pi(n+n_o)\bar{k}}{N}}}_{\text{ICI}}$$
$$+ \underbrace{\frac{1}{N}\sum_{n=N-n_o}^{N-1}\sum_{\bar{k}=0}^{N-1} X_{m+1,k}\mathrm{e}^{\frac{j2\pi(n-N-N_{cp}+n_o)\bar{k}}{N}}\mathrm{e}^{\frac{-j2\pi n_o k}{N}}}_{\text{ISI}}. \tag{6.9}$$

6.5.2 EFFECT OF CARRIER FREQUENCY OFFSET

The carrier-frequency offset (CFO) refers to the mismatch between the frequency of the received signal and the frequency of the local oscillator at the receiver. Two factors contribute to the CFO: i) the frequency mismatch between the transmitter and the receiver oscillators; ii) the Doppler effect due to the relative mobility of the transmitter and the receiver. In practice, the oscillators at the transmitter and the receiver can never oscillate at identical frequencies; therefore, there always exists a CFO in the received baseband signal. Due to the CFO, the baseband signal is shifted in the frequency domain. As we go higher in carrier frequencies, the CFO is more pronounced due to both the oscillator frequency mismatch and the Doppler effect.

Multicarrier waveforms are more sensitive to the CFO than single-carrier waveform, since a subcarrier bandwidth is typically much smaller than the overall bandwidth in multicarrier waveforms. A small CFO can cause significant degradation in the symbol error rate performance. In an OFDM system, the CFO produces two effects: i) a common phase error (CPE), ii) an intercarrier interference (ICI). The CPE refers to a common phase rotation in all subcarriers and the ICI refers to an interference between the subcarriers due to the loss of subcarrier orthogonality. Let us define the CPE and the ICI, mathematically. Consider a received baseband signal subject to the CFO: $r[n] = x[n]\mathrm{e}^{j2\pi\frac{\epsilon}{N}n}$, where ϵ is a normalized fractional CFO. The demodulation of the subcarrier l is then given by

$$\begin{aligned}
R_l &= \frac{1}{N}\sum_{n=0}^{N-1} r[n]\mathrm{e}^{-j2\pi\frac{l}{N}n} \\
&\overset{(a)}{=} \frac{1}{N}\sum_{n=0}^{N-1}\sum_{i=0}^{N-1} X_i\mathrm{e}^{j2\pi\frac{i}{N}n}\mathrm{e}^{-j2\pi\frac{l}{N}n}\mathrm{e}^{j2\pi\frac{\epsilon}{N}n} \\
&= X_l\frac{1}{N}\sum_{n=0}^{N-1}\mathrm{e}^{j2\pi\frac{\epsilon}{N}n} + \sum_{n=0}^{N-1}\sum_{i=0,i\neq l}^{N-1} X_i\mathrm{e}^{j2\pi\frac{i-l+\epsilon}{N}n} \\
&\overset{(b)}{=} \alpha X_l\underbrace{\mathrm{e}^{j\pi\epsilon\frac{N-1}{N}}}_{\text{CPE}} + \underbrace{\sum_{n=0}^{N-1}\sum_{i=0,i\neq l}^{N-1} X_i\mathrm{e}^{j2\pi\frac{i-l+\epsilon}{N}n}}_{\text{ICI}_l},
\end{aligned} \tag{6.10}$$

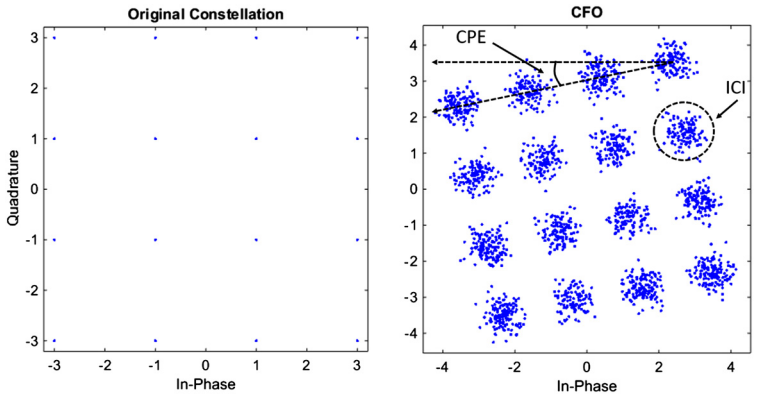

FIGURE 6.23

Effects of carrier-frequency offset in an OFDM system.

where α is an attenuation factor common to all subcarriers, which is given by

$$\alpha = \frac{sinc\,(\epsilon)}{sinc\,(\epsilon/N)}. \tag{6.11}$$

As an example, the two effects produced by CFO in an OFDM system (CPE and ICI) are illustrated in Fig. 6.23 for a 16-QAM constellation. CPE causes an identical phase rotation in all subcarriers within an OFDM symbol and ICI acts as an additive noise in the demodulated subcarrier. CPE can easily be compensated for as part of the channel equalization process. Assuming perfect CPE compensation, the achievable signal-to-interference ratio (SIR) due to ICI in the demodulated subcarrier l in the OFDM symbol subject to CFO is given by

$$\mathrm{SIR}_l = \frac{\alpha^2 E\left[|X_l|^2\right]}{E\left[|\mathrm{ICI}_l|^2\right]}, \tag{6.12}$$

where $E[\cdot]$ is the expectation operator.

6.5.3 SAMPLING FREQUENCY OFFSET

The sampling frequency offset (SFO) refers to a mismatch between the oscillator of the transmitter and the oscillator of the receiver. In practice, the sampling clocks of the transmitter and the receiver are offset by a few parts per million (ppms), which can cause major degradation in an OFDM system if not properly compensated for. In the following, we briefly discuss the effect of the SFO in an OFDM system.

Consider an OFDM transmitter with the sampling time T_T and an associated OFDM receiver with the sampling time T_R (i.e., assuming that the sampling rates are not identical). Then the received baseband OFDM signal can be expressed as $\sum_{i=0}^{N-1} X_i e^{j2\pi in\frac{T_R}{T_T}}$. Let us define $\eta := \frac{T_R - T_T}{T_T}$. The de-

modulation of a subcarrier l is then given by

$$\begin{aligned} R_l &= \frac{1}{N}\sum_{n=0}^{N-1} r[n]\mathrm{e}^{-j2\pi\frac{l}{N}n} \\ &= \frac{1}{N}\sum_{n=0}^{N-1}\sum_{i=0}^{N-1} X_i \mathrm{e}^{j2\pi in\frac{T_R}{T_T}}\mathrm{e}^{-j2\pi l\frac{n}{N}} \\ &= X_l\sum_{n=0}^{N-1}\mathrm{e}^{-j2\pi ln\frac{(T_R-T_T)}{T_T N}} + \sum_{n=0}^{N-1}\sum_{i=0,i\neq l}^{N-1} X_i \mathrm{e}^{j2\pi n\frac{iT_R-lT_T}{T_T N}} \\ &= \alpha_l X_l \underbrace{\sum_{n=0}^{N-1}\mathrm{e}^{j\pi l\eta\frac{N-1}{N}}}_{\text{linear phase drift}} + \underbrace{\sum_{n=0}^{N-1}\sum_{i=0,i\neq l}^{N-1} X_i \mathrm{e}^{j2\pi\frac{i-l+\epsilon}{N}n}}_{\text{ICI}}, \end{aligned} \tag{6.13}$$

where α_l is given by

$$\alpha_l = \frac{sinc\,(l\eta)}{sinc\,(l\eta/N)}. \tag{6.14}$$

From (6.13), we observe that the SFO induces a linear phase drift across the subcarriers in contrast to CFO that produces a common phase rotation (CPE) in all subcarriers. Moreover, different subcarriers are also attenuated differently when subject to the SFO, unlike the CFO. Typically, the ICI term due to the SFO is very small and can be neglected.

6.6 IMPAIRMENT MITIGATION

We have seen that an OFDM system is sensitive to the phase-noise, the carrier-frequency offset, and the sampling frequency offset. NR is expected to be deployed at frequencies as high as 100 GHz, where these impairments would be a major bottleneck. In this section, we discuss mitigation schemes for these impairments assuming a slow time varying frequency-selective channel. In a fast varying channel, these impairments are typically corrected as part of the channel estimation and equalization process.

6.6.1 A PHASE-NOISE MITIGATION SCHEME

In order to focus on the PN impairment, we assume a perfect time-synchronization and a quasi-static multipath channel (with a channel length of L samples). The PN impaired signal at the receiver at the nth time sample can be expressed as

$$y[n] = \exp\left(j\phi[n]\right)\sum_{l=0}^{L-1} h_l x[n-l] + w[n], \tag{6.15}$$

where $x[n]$ represents the transmitted OFDM signal including the CP, h_l ($l = 0, \cdots, L\text{-}1$) is the lth tap of the channel impulse response (CIR), $w[n]$ denotes the additive white Gaussian noise (AWGN), and $\phi[n]$ denotes the PN.

Let $\mathbf{y} = \left[y[0]\ y[1]\ \cdots\ y[N-1]\right]^T$ be the received time-domain OFDM symbol (after CP removal), where N is the number of subcarriers. The PN is mitigated by the operation $\mathbf{\Phi y}$, where

$$\mathbf{\Phi} = \text{diag}\left\{\left[\exp\left(-j\hat{\phi}\,[0]\right)\ \cdots\ \exp\left(-j\hat{\phi}\,[N-1]\right)\right]^T\right\}, \tag{6.16}$$

with $\hat{\phi}$ denoting the estimate of ϕ. Hence, the task of the PN mitigation scheme is to essentially estimate the PN samples.

Let $\mathbf{H}_\text{p}$ be an $N_\text{p} \times N_\text{p}$ diagonal matrix consisting of the channel transfer functions (CTFs) at the N_p pilot subcarriers ($N_\text{p} \leq N$), $\mathbf{s}_\text{p}$ be a vector consisting of the N_p subcarriers, $\mathbf{D}$ be an $N_\text{p} \times N$ submatrix of the $N \times N$ discrete Fourier transform (DFT) matrix $\mathbf{F}$ (whose elements are given by $\exp(-j2\pi nk/N)/\sqrt{N}$ with $k,\ n \in \{0, \cdots, N-1\}$) corresponding to the N_p pilot subcarriers, and $\tilde{\mathbf{w}}$ be an $N \times 1$ vector consisting of the time-domain AWGNs. We have

$$\mathbf{D\Phi y} = \mathbf{H}_\text{p}\mathbf{s}_\text{p} + \mathbf{D\Phi}\tilde{\mathbf{w}}. \tag{6.17}$$

Let $\mathbf{Y} = \text{diag}(\mathbf{y})$ and $\mathbf{T}$ be an $N \times q$ transformation matrix, such that $\mathbf{\Phi} \approx \text{diag}(\mathbf{T}\boldsymbol{\alpha})$, where $\boldsymbol{\alpha}$ consists of q unknowns or anchors ($q \leq N_\text{p}$), and it is given by

$$\boldsymbol{\alpha} = (\mathbf{DYT})^\dagger\,\mathbf{H}_\text{p}\mathbf{s}_\text{p} + (\mathbf{DYT})^\dagger\,\tilde{\mathbf{w}}. \tag{6.18}$$

The first term in the right hand side (RHS) of (6.18) is the least-square (LS) estimator of $\boldsymbol{\alpha}$, whereas the second term in the RHS of (6.18) is additive noise.

The physical meaning of $\boldsymbol{\alpha}$ depends on the type of the transformation matrix. If $\mathbf{T}$ is a linear interpolation matrix [5], the elements in $\boldsymbol{\alpha}$ are estimates of the inverse carrier PN $\exp(-j\phi)$ at the q anchors (time samples). These anchors are usually evenly distributed in the time-domain OFDM symbol.

Typically, the phase-noise power is concentrated in low frequencies. As an example, the power spectral density (PSD) of mmMAGIC phase-noise model at 82 GHz is shown in Fig. 6.24 [7]. As phase noise is dominant in lower frequencies, $\mathbf{T}$ can be a $N \times q$ submatrix of $\mathbf{F}$ corresponding to the q lowest spectral components. In this case, the elements in $\boldsymbol{\alpha}$ are the spectral components of $\exp(-j\phi)$.

The computational complexity of the PN mitigation scheme mainly depends on the pseudoinverse of an $N_\text{p} \times q$ matrix in (6.18), whose complexity increases linearly with N_p, yet cubically with q [2].

For convenience of the analysis, we study the performance of the PN mitigation/estimation in the preamble (where $N_\text{p} = N$). (The findings hold for the payload as well, where $N_\text{p} < N$.)

The LS estimator of the PN, i.e., the first term in the RHS of (6.18), contains the modeling error $\mathbf{\Phi} - \text{diag}(\mathbf{T}\boldsymbol{\alpha})$. Assuming perfect estimation of $\boldsymbol{\alpha}$ (by setting the second term in the RHS of (6.18), i.e., the additive noise, to zero), it is self-evident that the modeling error reduces to zero as q increases to N.

Now we examine the effect of the additive noise in (6.18) w.r.t. q. Let $\breve{\mathbf{w}} = \mathbf{F\Phi}\tilde{\mathbf{w}}$. Since $\mathbf{F\Phi}$ is a unitary matrix, $\breve{\mathbf{w}}$ and $\tilde{\mathbf{w}}$ have the same statistics. Thus, the additive noise in (6.18) can be equivalently written as

$$\mathbf{z} = (\mathbf{FYT})^\dagger\,\breve{\mathbf{w}} = (\mathbf{T})^\dagger\,(\mathbf{Y})^{-1}\,(\mathbf{F})^H\,\tilde{\mathbf{w}}. \tag{6.19}$$

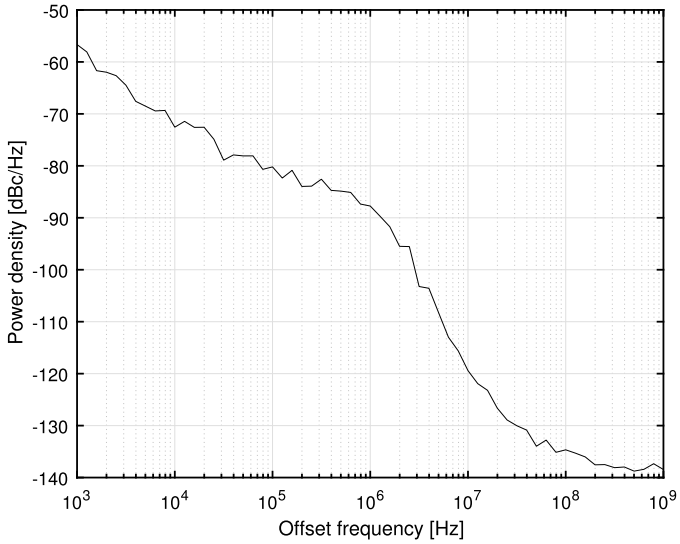

FIGURE 6.24

PSD of phase-noise.

For simplicity, we assume that $\mathbf{T}$ is the DFT transformation matrix. The power of the additive noise is given as

$$\begin{aligned}
\mathrm{E}\left[\mathbf{z}^H\mathbf{z}\right] &= \sigma_w^2 \mathrm{E}\left\{\mathrm{Tr}\left[(\mathbf{T})^\dagger (\mathbf{Y})^{-1}\left((\mathbf{Y})^{-1}\right)^*\left((\mathbf{T})^\dagger\right)^H\right]\right\} \\
&= \sigma_w^2 \mathrm{E}\left\{\mathrm{Tr}\left[\left(\mathbf{T}\mathbf{T}^H\right)^\dagger (\mathbf{Y})^{-1}\left((\mathbf{Y})^{-1}\right)^*\right]\right\} \\
&\geq \frac{q}{N}\frac{\sigma_w^2}{\sigma_h^2\sigma_s^2+\sigma_w^2} = \frac{q}{N}\frac{1}{\gamma_0+1},
\end{aligned} \tag{6.20}$$

where the last inequality follows from the Jensen's inequality and by denoting σ_h^2, σ_s^2, and σ_w^2 as variances of the CIR, subcarrier symbol, and AWGN, respectively; and $\gamma_0 = \sigma_h^2\sigma_s^2/\sigma_w^2$ is the signal-to-noise ratio (SNR). As can be seen, increasing q will increase the power of the additive noise in (6.18) for fixed N and SNR. This is because there are more anchors to the estimate as q increases. All in all, for the PN estimation, increasing q reduces the modeling error, yet increases the additive noises. As mentioned before, the computational complexity of the PN estimation increases cubically with increasing q. Therefore, q should not be unnecessarily large. For example, it has been shown that $q = 7$ is sufficient for mitigating the PN [4].

For simulations, we assume a DFT size of 512, including 32 scattered pilots. The remaining active subcarriers are loaded with 16- or 64-QAM. The CP length is set to be larger than the channel length. The sampling frequency is set so that the subcarrier spacing is 240 or 480 kHz. The carrier frequency

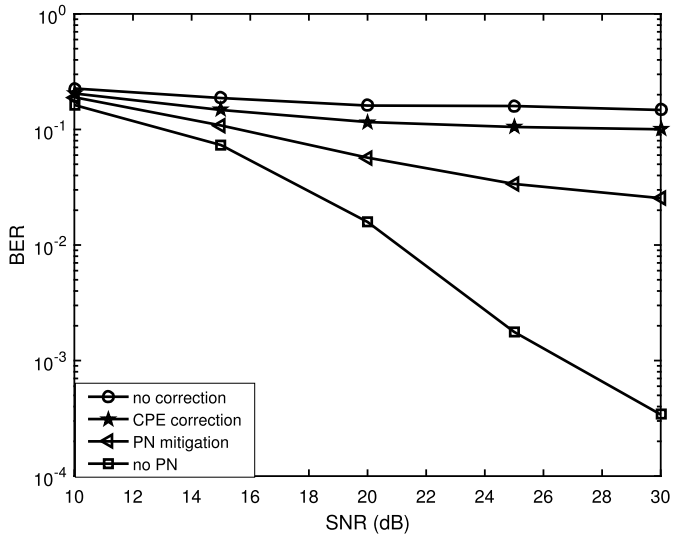

FIGURE 6.25

SER performance with 240 kHz subcarrier spacing and 64-QAM.

is set to fc = 82 GHz. The QuaDRiGa channel model [9] is used for channel emulation. Both the CPE correction [17] and the PN mitigation scheme with $q = 7$ are evaluated. Figs. 6.25–6.27 show the BER performances with/without phase-noise compensations with 16- and 64-QAM, and 240 and 480 kHz subcarrier spacing. It can be seen that the phase-noise mitigation scheme clearly outperforms the CPE correction (at the expense of increased complexity); and the corresponding BER performance improves as the subcarrier spacing increases from 240 to 480 kHz and as the modulation order decreases from 64-QAM to 16-QAM.

6.6.2 CFO AND SFO MITIGATION

In this section, we discuss estimation (and correction) of the CFO and the SFO. A scheme for mitigation of the SFO and the CFO (jointly with PN) is presented. This is an extension of the PN mitigation scheme presented in Section 6.6.1.

There exists an extensive literature on mitigation of the synchronization errors in OFDM systems. Thanks to the seminal work on the CFO estimation [16], [15], the (coarse) frequency synchronization can be readily achieved and our focus will be on the residual carrier-frequency offset estimation. The SFO mitigation is studied in [3], [19]. A pilot-based SFO estimator is proposed in [3], which estimates the SFO using scattered pilots in each OFDM symbol. The SFO can also be tracked using a delay-locked loop (DLL) [18]. A blind SFO estimator is proposed in [19], which estimates the SFO using current and previously received OFDM symbols. In general, the pilot-based SFO estimator outperforms the blind estimator and because the scattered pilots are needed for the PN estimation, the pilot-based SFO estimator is more popular in practical systems. To be robust to perturbations from an imperfect

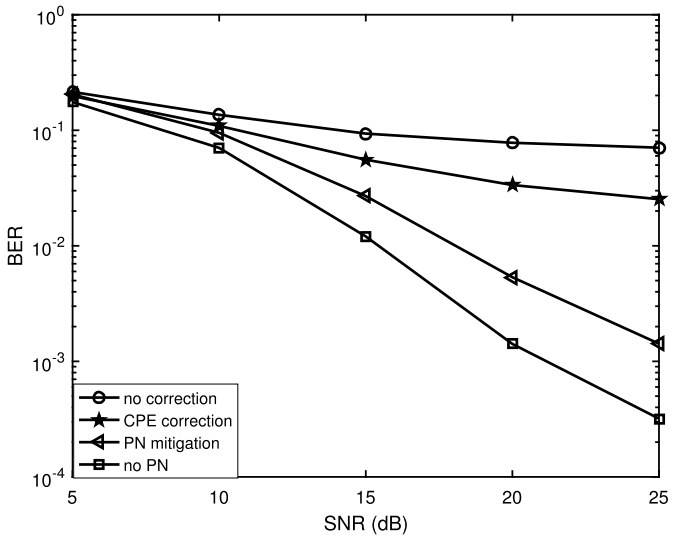

FIGURE 6.26

SER performance with 480 kHz subcarrier spacing and 64-QAM.

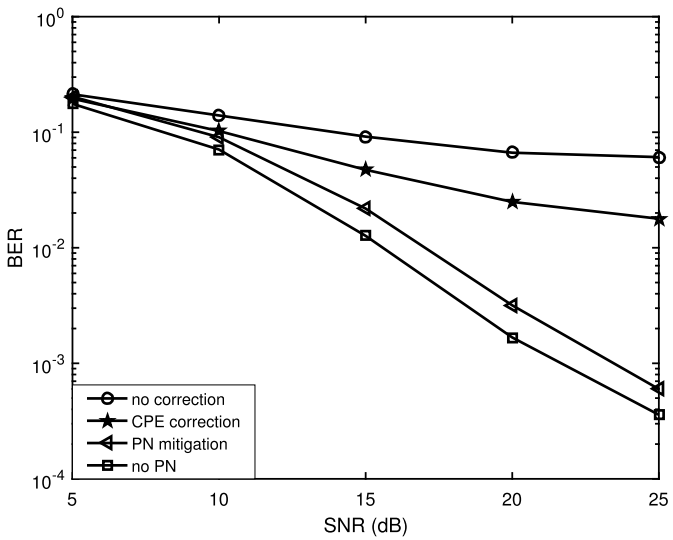

FIGURE 6.27

SER performance with 480 kHz subcarrier spacing and 16-QAM.

PN mitigation, ICI, and AWGN, the pilot-based SFO estimator can be combined with the Kalman filter to track the SFO. Unlike the DLL, the Kalman filter can also be used for channel prediction, which is necessary for the PN mitigation (prior to the SFO correction).

In the following, we present a mitigation scheme for the CFO and the SFO, assuming that there is a single clock and a single oscillator in the transmitter/receiver. For the case of multiple oscillators per transceiver, the interested reader may refer to [13], [6]. For simplicity and without loss of generality, we assume that coarse frequency synchronization has been achieved using the classical CFO estimation ([16,15]) with a residual CFO (RCFO) of ε. The residual CFO (RCFO) is normalized to the sampling frequency. Let T_{T} and T_{R} be the sampling intervals at the transmitter and at the receiver, respectively. The SFO can then be expressed as

$$\eta = \frac{T_{\mathrm{R}} - T_{\mathrm{T}}}{T_{\mathrm{T}}}. \tag{6.21}$$

The SFO is introduced to the transmit signal by sequentially sending the OFDM symbols to a buffer (which is longer than the duration of one OFDM symbol with CP), and sampling the buffered signal using the windowed sinc interpolation function with a sampling interval of $T_{\mathrm{T}}(1-\eta)$.

Consider the PN mitigation scheme presented in Section 6.6.1 with $\hat{\phi}[n]$ now denoting the estimate of the PN plus the RCFO at nth time sample,

$$\hat{\phi}[n] \approx \phi[n] + 2\pi\varepsilon n. \tag{6.22}$$

Once $\hat{\phi}[n]$ is estimated, the RCFO can be approximated by

$$\hat{\varepsilon} \approx \frac{1}{2\pi N} \sum_{n=0}^{N-2} \left(\hat{\phi}[n+1] - \hat{\phi}[n] \right). \tag{6.23}$$

The above expression assumes that the time derivative of the PN has zero mean, which holds for practical oscillators. After the PN mitigation, the RCFO becomes $\tilde{\varepsilon} \approx \varepsilon - \hat{\varepsilon}$.

The SFO causes a phase rotation (which varies linearly across subcarriers) and ICI. SFO is typically just a few ppm in practical systems; thus, the resulting ICI is negligible. For notational convenience, we drop the ICI term caused by the SFO in the following expressions. The received signal of the mth OFDM symbol at the kth subcarrier is given by

$$r_m[k] = J_m[0]\exp\left(j\frac{k\psi_m}{N}\right) H_m[k]s_m[k] + \sum_{l=0, l\neq k}^{N-1} J_m[k-l]\exp\left(j\frac{l\psi_m}{N}\right) H_m[l]s_m[l] + w_m[k], \tag{6.24}$$

where $s_m[k]$ and $r_m[k]$ are transmitted and received signals, $J_m[k]$ is the spectral component of the phase noise together with the RCFO (after PN mitigation), ψ_m is the rotation angle caused by the SFO together with the RCFO, $H_m[k]$ is the channel transfer function, and $w_m[k]$ is the AWGN. We have

$$J_m[k] = \frac{1}{N} \sum_{n=0}^{N-1} \exp\left(j\left(\tilde{\phi}_m[n] + 2\pi\tilde{\varepsilon}n\right)\right) \exp\left(-\frac{2\pi kn}{N}\right), \tag{6.25}$$

$$\psi_m = 2\pi m(N + N_g)\,(N\tilde{\varepsilon}/k + \eta)\,, \tag{6.26}$$

where $\tilde{\phi}_m[n]$ is the residual PN after the PN mitigation at the nth time sample of the mth OFDM symbol, and N_g denotes the CP length of the OFDM symbol. As can be seen, μ_m varies linearly over the OFDM symbol time. After an effective PN mitigation, $J_m(0)$ is close to one and the ICI term (i.e., the second term in (6.24)) is close to zero. Let $\tilde{H}_m[k] = J(0)H_m[k]$ and $\tilde{w}_m[k]$ be the sum of the ICI and AWGN terms, Eq. (6.24) can then be rewritten as

$$r_m[k] = \exp\left(j\frac{k\psi_m}{N}\right)\tilde{H}_m[k]s_m[k] + \tilde{w}_m[k]. \tag{6.27}$$

The (frequency-domain) phase rotation ψ_m must be corrected prior to the data detection. To be robust to perturbations of the residual PN and the AWGN, we apply the Kalman filter to track ψ_m. Let δ_m be the time derivative of ψ_m. The state-space model is given as

$$\mathbf{s}_{m+1} = \mathbf{M}\mathbf{s}_m + \mathbf{n}, \tag{6.28}$$

where $\mathbf{s}_m = [\psi_m\ \delta_m]^T$, $\mathbf{n}$ denotes the 2×1 state model noise vector, and

$$\mathbf{M} = \begin{bmatrix} 1 & 1 \\ 0 & 1 \end{bmatrix}.$$

The covariance matrix of $\mathbf{n}$ is denoted $\mathbf{Q} = E[\mathbf{n}\mathbf{n}^H]$, where E is the expectation operator. The observation model is

$$\mu_m = \psi_m + \zeta, \tag{6.29}$$

where ζ denotes the observation noise with a variance of $\kappa = E[\zeta\zeta^*]$. By denoting the observation vector as $\mathbf{o} = [1\ 0]^T$; we can write

$$\mu_m = \mathbf{o}^T\mathbf{s}_m + \zeta. \tag{6.30}$$

The Kalman filter algorithm is now given by:

Initialize:

$$\begin{aligned} \mathbf{s}_{0|0} &= \begin{bmatrix} 0 & 0 \end{bmatrix}^T \\ \mathbf{P}_{0|0} &= \mathbf{I}_2. \end{aligned} \tag{6.31}$$

Iterate:

predict:

$$\begin{aligned} \mathbf{s}_{m|m-1} &= \mathbf{M}\mathbf{s}_{m-1|m-1} \\ \mathbf{P}_{m|m-1} &= \mathbf{M}\mathbf{P}_{m-1|m-1}\mathbf{M}^T + \mathbf{Q} \end{aligned} \tag{6.32}$$

update:

$$\begin{aligned}
\alpha_m &= \mu_m - \mathbf{o}^T \mathbf{s}_{m|m-1} \\
\mathbf{k}_m &= \frac{\mathbf{P}_{m|m-1}\mathbf{o}}{\mathbf{o}^T \mathbf{P}_{m|m-1}\mathbf{o}} \\
\mathbf{s}_{m|m} &= \mathbf{s}_{m|m-1} + \mathbf{k}_m \alpha_m \\
\mathbf{P}_{m|m} &= (\mathbf{I}_2 - \alpha_m \mathbf{k}_m)\, \mathbf{P}_{m|m-1}.
\end{aligned} \tag{6.33}$$

At the mth OFDM symbol time, the phase rotation has to be estimated based on the scattered pilots in the mth OFDM symbol. Let k_p $(p = 1,\ ...,\ N_\mathrm{p})$ be the indices of the N_p pilots in the mth OFDM symbol, and denote

$$\vartheta_m[k] = \angle \left(\frac{\left(\tilde{H}_m[k] s_m[k]\right)^* r_m[k]}{\left(\tilde{H}_m[k] s_m[k]\right)^* \left(\tilde{H}_m[k] s_m[k]\right)} \right), \tag{6.34}$$

where $\angle(\cdot)$ denotes the angle of its argument, and the superscript * denotes the complex conjugate operation. The phase rotation can be estimated as

$$\mu_m = \frac{N}{N_\mathrm{p} - 1} \sum_{p=1}^{N_\mathrm{p}-1} \frac{\vartheta_m[k_p] - \vartheta_m[k_{p+1}]}{k_p - k_{p+1}}. \tag{6.35}$$

When $|\mu_m|$ is larger than 2π, the synchronization module shifts the signal by one sample accordingly; otherwise, the SFO is corrected by $\exp(-jk\mu_m/N)\, \mathbf{y}_m[k]$. Note that the SFO correction also compensates for the RCFO $\tilde{\varepsilon}$. The PN mitigation and the SFO correction are applied to both the training signal and the payload. In the payload, the estimated channel is used together with the Kalman filter for the channel prediction. Specifically, we predict the phase rotation for the next OFDM symbol:

$$\mu_{m+1}[k] = \mathbf{o}^T \mathbf{M} \mathbf{s}_{m|m}. \tag{6.36}$$

The channel prediction for the next OFDM symbol is

$$\hat{H}_{m+1}[k] = \exp\left(\frac{jk\mu_{m+1}}{N}\right) \hat{H}_m[k], \tag{6.37}$$

which is used for the PN mitigation in the next OFDM symbol. We assume that the OFDM payload has 512 subcarriers, including 354 active subcarriers, 32 pilot subcarriers, and 158 guard band subcarriers (79 null subcarriers in the beginning and 79 at the end of each OFDM symbol). The guard band helps to reduce the out-of-band emission and eliminates the distortions in the interpolation and the decimation process. The CP length is set to be larger than the channel length. We further assume that the system is operating at 60 GHz with 256-QAM and sampling frequency 100 MHz. For tracking the frequency-domain phase rotation (due to the SFO and the RCFO) using the Kalman filter, we assume the covariance matrix of the state model noises to be $\mathbf{Q} = 10^{-15}\mathbf{M}\mathbf{M}^T$ and the variance of

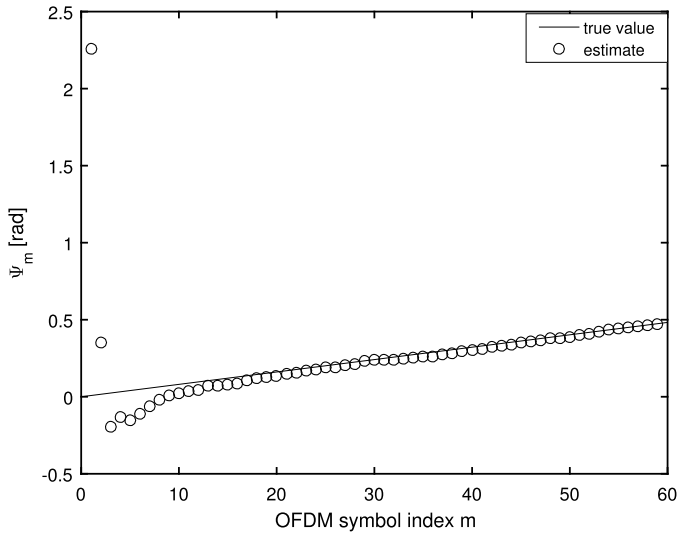

FIGURE 6.28

Example of the SFO phase rotation and its estimate as a function of the OFDM symbol index m.

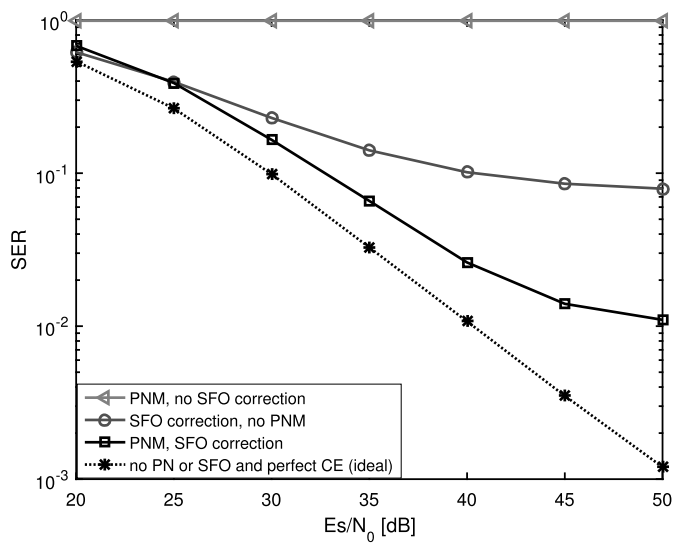

FIGURE 6.29

SER performances of the uncoded MIMO-OFDM system with/without the PN mitigation or the SFO correction in an urban microcell scenario at 60 GHz.

the observation noise to be $\kappa = 0.01$. Note that the small covariance matrix $\mathbf{Q}$ is justified by the time-invariant state model. The observation noise ζ is actually the estimation error of the phase rotation estimator, whose mean square error (MSE) is nontrivial to derive. However, it is found that the error rate performance of the system is insensitive to the value of κ (i.e., the variance of ζ) ranging from 0.001 to 0.1. Fig. 6.28 shows an example of the estimate of the phase rotation ψ_m and its true values as functions of the OFDM symbol index m. As can be seen, the estimates converge after the first eight OFDM symbols. Note that, apart from being robust to perturbations, e.g., of the PN estimation error, the Kalman filter is also used for the channel prediction for the PN mitigation.

For evaluating the error rate performance of the MIMO-OFDM link in a multipath fading channel, we resort to the QuaDRiGa channel model [9]. In total 200 drops are generated. For each channel drop, 10 preamble symbols and 50 payload symbols are transmitted. Fig. 6.29 shows the symbol error rate (SER) performance of the uncoded MIMO-OFDM system in the presence of the PN, the SFO, and the RCFO with/without the PN mitigation (PNM) and the SFO correction. For comparison, we also plot SERs for the ideal case without the PN, the SFO, the RCFO, and with a perfect channel estimation. As can be seen, the PN and SFO must be jointly compensated for in order to have an acceptable SER performance.

REFERENCES

[1] E. Bala, J. Li, R. Yang, Shaping spectral leakage: a novel low-complexity transceiver architecture for cognitive radio, IEEE Vehicular Technology Magazine 8 (3) (2013, Sept.) 38–46.

[2] P. Bürgisser, M. Clausen, A. Shokrollahi, Algebraic Complexity Theory, Springer-Verlag, Berlin/Heidelberg, 1997.

[3] D.C. Chang, Effect and compensation of symbol timing offset in ofdm systems with channel interpolation, IEEE Transactions on Broadcasting (ISSN 0018-9316) 54 (4) (2008, Dec.) 761–770, https://doi.org/10.1109/TBC.2008.2002339.

[4] X. Chen, OFDM based multi-node transmission in the presence of phase noises for small cell backhaul, IEEE Communications Letters (ISSN 1089-7798) 21 (5) (2017, May) 1207–1210, https://doi.org/10.1109/LCOMM.2017.2655509.

[5] X. Chen, A. Wolfgang, Phase noise mitigation in ofdm-based backhaul in the presence of channel estimation and synchronization errors, in: 2016 IEEE 83rd Vehicular Technology Conference (VTC Spring), 2016, May, pp. 1–5.

[6] X. Chen, C. Fang, Y. Zou, A. Wolfgang, T. Svensson, Beamforming mimo-ofdm systems in the presence of phase noises at millimeter-wave frequencies, in: 2017 IEEE Wireless Communications and Networking Conference Workshops (WCNCW), 2017, March, pp. 1–6.

[7] D5.1, Initial multi-node and antenna transmitter and receiver architectures and schemes, Millimetre-Wave Based Mobile Radio Access Network for Fifth Generation Integrated Communications (mmMAGIC), 2016.

[8] G. Huang, A. Nix, S. Armour, Impact of radio resource allocation and pulse shaping on PAPR of SC-FDMA signals, in: Proc. IEEE 18th International Symposium on Personal, Indoor and Mobile Radio Communications (PIMRC), 2007, Sept., pp. 1–5.

[9] S. Jaeckel, L. Raschkowski, K. Börner, L. Thiele, Quadriga: a 3-d multi-cell channel model with time evolution for enabling virtual field trials, IEEE Transactions on Antennas and Propagation (ISSN 0018-926X) 62 (6) (2014, June) 3242–3256, https://doi.org/10.1109/TAP.2014.2310220.

[10] D.W. Lim, S.J. Heo, J.S. No, An overview of peak-to-average power ratio reduction, Journal of Communications and Networks 11 (3) (2009, June) 229–239.

[11] A. Mehrotra, Noise analysis of phase-locked loops, in: IEEE/ACM International Conference on Computer Aided Design. ICCAD – 2000. IEEE/ACM Digest of Technical Papers (Cat. No.00CH37140), 2000, Nov., pp. 277–282.

[12] S.H. Muller-Weinfurtner, Optimum Nyquist windowing in OFDM receivers, IEEE Transactions on Communications 49 (3) (2001, Mar.) 417–420.

[13] A. Puglielli, G. LaCaille, A.M. Niknejad, G. Wright, B. Nikolić, E. Alon, Phase noise scaling and tracking in OFDM multi-user beamforming arrays, in: 2016, IEEE International Conference on Communications (ICC), 2016, May, pp. 1–6.

[14] R1-162960, Summary of email discussion on link level channel model, 3GPP TSG RAN WG1 Meeting 84b, 2016, April.

[15] T.M. Schmidl, D.C. Cox, Robust frequency and timing synchronization for ofdm, IEEE Transactions on Communications (ISSN 0090-6778) 45 (12) (1997, Dec.) 1613–1621, https://doi.org/10.1109/26.650240.
[16] J.J. van de Beek, M. Sandell, P.O. Borjesson, Ml estimation of time and frequency offset in OFDM systems, IEEE Transactions on Signal Processing (ISSN 1053-587X) 45 (7) (1997, July) 1800–1805, https://doi.org/10.1109/78.599949.
[17] S. Wu, Y. Bar-Ness, OFDM systems in the presence of phase noise: consequences and solutions, IEEE Transactions on Communications (ISSN 0090-6778) 52 (11) (2004, Nov.) 1988–1996, https://doi.org/10.1109/TCOMM.2004.836441.
[18] B. Yang, K.B. Letaief, R.S. Cheng, Z. Cao, Timing recovery for OFDM transmission, IEEE Journal on Selected Areas in Communications (ISSN 0733-8716) 18 (11) (2000, Nov.) 2278–2291, https://doi.org/10.1109/49.895033.
[19] Y.H. You, S.T. Kim, K.T. Lee, H.K. Song, An improved sampling frequency offset estimator for ofdm-based digital radio mondiale systems, IEEE Transactions on Broadcasting (ISSN 0018-9316) 54 (2) (2008, June) 283–286, https://doi.org/10.1109/TBC.2008.915763.
[20] A.A. Zaidi, R. Baldemair, H. Tullberg, H. Bjorkegren, L. Sundstrom, J. Medbo, C. Kilinc, I.D. Silva, Waveform and numerology to support 5G services and requirements, IEEE Communications Magazine (ISSN 0163-6804) 54 (11) (2016, November) 90–98, https://doi.org/10.1109/MCOM.2016.1600336CM.
[21] J. Zhang, C. Huang, G. Liu, P. Zhang, Comparison of the link level performance between OFDMA and SC-FDMA, in: Communications and Networking in China (ChinaCom), 2006, Oct., pp. 1–6.